7832–7850 *Nucleic Acids Research, 2023, Vol. 51, No. 15* *Published online 5 July 2023*
https://doi.org/10.1093/nar/gkad571

RNA polymerase common subunit ZmRPABC5b is transcriptionally activated by Opaque2 and essential for endosperm development in maize

Quanquan Chen [1,2], Yingmei Guo[1], Jie Zhang [1], Nannan Zheng[1], Jie Wang[1], Yan Liu [2], Jiawen Lu[1], Sihan Zhen[1], Xuemei Du[1], Li Li[1], Junjie Fu [2], Guoying Wang [2], Riliang Gu [1,*], Jianhua Wang [1,*] and Yunjun Liu [2,*]

[1]Beijing Innovation Center for Crop Seed Technology, Ministry of Agriculture and Rural Affairs; State Key Laboratory of Maize Bio-breeding; Center for Seed Science and Technology, College of Agronomy and Biotechnology, China Agricultural University, Beijing 100193, China and [2]Institute of Crop Sciences, Chinese Academy of Agricultural Sciences, Beijing 100081, China

Received January 06, 2023; Revised June 08, 2023; Editorial Decision June 13, 2023; Accepted June 24, 2023

ABSTRACT

Maize (*Zea mays*) kernel size is an important factor determining grain yield; although numerous genes regulate kernel development, the roles of RNA polymerases in this process are largely unclear. Here, we characterized the *defective kernel 701* (*dek701*) mutant that displays delayed endosperm development but normal vegetative growth and flowering transition, compared to its wild type. We cloned *Dek701*, which encoded ZmRPABC5b, a common subunit to RNA polymerases I, II and III. Loss-of-function mutation of *Dek701* impaired the function of all three RNA polymerases and altered the transcription of genes related to RNA biosynthesis, phytohormone response and starch accumulation. Consistent with this observation, loss-of-function mutation of *Dek701* affected cell proliferation and phytohormone homeostasis in maize endosperm. *Dek701* was transcriptionally regulated in the endosperm by the transcription factor Opaque2 through binding to the GCN4 motif within the *Dek701* promoter, which was subjected to strong artificial selection during maize domestication. Further investigation revealed that DEK701 interacts with the other common RNA polymerase subunit ZmRPABC2. The results of this study provide substantial insight into the Opaque2–*ZmRPABC5b* transcriptional regulatory network as a central hub for regulating endosperm development in maize.

GRAPHICAL ABSTRACT

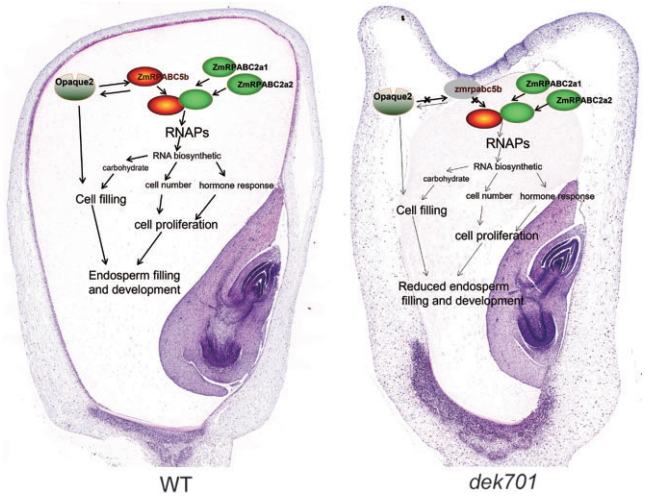

INTRODUCTION

Transcription is a basic cellular process that involves transcribing genetic information from DNA to many RNA copies in each cell. DNA-dependent RNA polymerases (RNAPs) are the main enzymes responsible for transcription in prokaryotes and eukaryotes (1,2). Eukaryotes possess three major types of RNAPs named RNA polymerase (Pol) I, II and III. Pol I synthesizes ribosomal RNA (rRNA); Pol II transcribes protein-coding genes into messenger RNAs (mRNAs), as well as many noncoding RNAs (ncRNAs); Pol III produces transfer RNAs (tRNAs) and other small ncRNAs including 5S rRNA and U6 small nuclear RNAs (3–5). Prokaryotes utilize only a single type of

*To whom correspondence should be addressed. Tel : +86 10 82105174; Email: liuyunjun@caas.cn
Correspondence may also be addressed to Jianhua Wang.Tel: +86 10 62732263; Email: wangjh63@cau.edu.cn
Correspondence may also be addressed to Riliang Gu.Tel: +86 10 62733853; Email: rilianggu@cau.edu.cn

RNAP for transcription (6,7). RNAPs are multi-subunit enzymes, with different subunits involved in catalysis, assembly or with auxiliary functions. Prokaryotic RNAP is composed of five core subunits: two catalytic subunits (β/β'), two homodimeric assembly subunits (α/α), and one auxiliary subunit (ω) (8–10). Eukaryotic Pol I, II and III complexes consist of 14, 12 and 17 subunits, respectively, and they share a conserved core of 12 subunits that includes 5 subunits to common all three polymerases (RNA Pol subunit ABC1 [RPABC1], RPABC2, RPABC3, RPABC4 and RPABC5) and 7 additional subunits that are distinct but paralogous across RNAPs (11).

RNAPs are at the core of all cellular and developmental processes, particularly during cell-cycle progression and organ development. For instance, yeast (*Saccharomyces cerevisiae*) *RPC53* encodes a subunit of Pol III, whose loss-of-function mutation leads to a predominantly G1 arrest (12). In mice (*Mus musculus*), mutation of the Pol III subunit Polr3b decreases cell proliferation in intestinal crypts during early postnatal development (13). In zebrafish (*Danio rerio*), a mutation in RPC2 caused a delay in the G1–S transition in highly proliferative tissues, such as the liver, retina, and terminal branchial arches (14). In plants, the Arabidopsis (*Arabidopsis thaliana*) Pol II subunit RPB1 plays a role in the maintenance of stem cell niches and cell-cycle control (15), while RPB3 (also named NRPB3, for the third largest subunit of nuclear Pol II) is essential for stomatal patterning and differentiation (16). In rice (*Oryza sativa*), the Pol III subunit C53 interacts with the transcription factor GRAIN LENGTH6 (GL6) to regulate the expression of genes involved in rice grain development (17). In maize (*Zea mays*), the Pol III subunit NRPC2 interacts with subunits RPC53 and AC40 and the transcription factor Floury3 (Fl3) to regulate Pol III activity during kernel development and storage reserve filling (18,19). The existence of subunits common to all three RNAPs indicates the tight coordination between RNAP functions. In yeast, the common subunits RPABC1, RPABC2, RPABC3 and RPABC5 are each essential for cell viability (20,21). Compared to the functional clues reported for non-common subunits, functions for common subunits are largely unknown.

Maize is an important crop that serves as a model plant for research on kernel development. Although numerous genes regulate kernel development in maize (22–29), how RNAPs might contribute to kernel development is unknown. However, two recent reports revealed the important roles of Pol III in maize kernel development. Maize Fl3 can interact with Pol III subunit RPC53 and the transcription factor C1, and the *fl3* mutant exhibits small and floury endosperm (18). In addition, a mutation in *NRPC2*, which is the second largest subunit of Pol III, disrupts Pol III activity and affects the expression of genes involved in cell proliferation, impairing maize kernel development (19). Despite these findings, little is known about the function of common RNAP subunits in plants and how the RNAP-encoding genes themselves might be regulated during kernel development.

In this study, we characterized the maize *defective kernel* (*dek*) mutant *dek701*. We cloned *Dek701* and report here that it encodes the RNA polymerase common subunit ZmRPABC5b. Loss-of-function mutation of *Dek701* impaired the function of all three types of RNAPs, affecting the transcription of genes related to RNA biosynthesis, phytohormone responses, cell-cycle progression and starch accumulation, as well as the transcription of rRNA, tRNAs and ncRNAs. We also discovered that DEK701 interacts with the other common subunit ZmRPABC2, and that *Dek701* transcription is regulated by Opaque2. These results revealed that the activation of *Dek701* transcription by Opaque2 is integral to coordinating transcription and endosperm growth at the grain filling stage, providing new insight into the regulatory mechanism of endosperm filling in maize.

MATERIALS AND METHODS

Plant materials

dek701 was isolated as a spontaneous mutant after multiple rounds of self-pollination from the progeny of a hybrid plant derived from a cross between inbred lines Chang7-2 and G38. The heterozygous *dek701* was self-pollinated to produce F_2 ears, from which WT and *dek* kernels were used for phenotype analysis. The *dek701* was crossed to B73, Zheng58, Chang7-2 and Mo17 inbred lines to produce segregating populations for genetic analysis, and the BC_4F_2 populations crossed to B73 were used for RNA-seq analysis. All plants were grown in Beijing (summer) and Hainan (winter), China.

Quantification of starch and protein contents

Twenty mature WT or mutant kernels were collected from the same ear. Endosperm was separated from the embryo and pericarp and pulverized with a mortar in liquid nitrogen. The resulting powder was collected after being freeze-dried with Labconco FreeZone 18 (Labconco Corporation, Kansas, MO, USA) until the weight stopped decreasing, then the powder was weighed and recorded. Starch was extracted and measured in 100 mg of powdered sample using an amyloglucosidase/a-amylase starch assay kit (Megazyme, Bray, Ireland).

Total protein, zein, and nonzein proteins were extracted from 50 mg of dried endosperm flour, according to the method of Wallace (30). Briefly, 1 ml petroleum ether was added into 50 mg powder, and the mixture was oscillated and incubated at 4°C for 1 h; the mixture was centrifuged at 13 000 rpm for 10 min, then the supernatant was discarded, and the precipitate was drained by FreeZone 18 Freeze Dryer. The precipitate was added with 1 ml of 12.5 mM sodium borate, 20 μl of 2% mercaptoethanol, and incubated overnight in a shaker at 37°C. The mixture was centrifuged at 13 000 rpm for 10 min, and the supernatant was the total protein extract. To isolate zein and nonzein proteins, 300 μl of total protein was mixed with 700 μl of anhydrous ethanol, and incubated at room temperature for more than 2 h. The mixture was centrifuged at 13 000 rpm for 10 min, then the supernatant was drained by FreeZone 18 as zein protein, and the precipitate consisted of nonzein proteins.Quantification analyses of the total protein, zein, and nonzein proteins were performed as described by Smith (31) using an Easy II protein quantitative kit (Transgen Biotech,

Beijing, China). SDS-PAGE was performed in 12% polyacrylamide gels, and the gels were stained with Coomassie brilliant blue R250 (32). All measurements were performed three times.

Light microscopy and SEM

Developing kernels were cut along their longitudinal axis. The samples were fixed for 3 days at room temperature in FAA solution (5 ml 38% [w/v] formaldehyde, 5 ml glacial acetic acid, 90 ml 70% [v/v] ethanol) and then embedded in paraffin after dehydration through a graded ethanol series (70% [v/v], 80%, 95% and 100% ethanol). Finally, the samples were cut into 8-μm sections, stained with 0.2% toluidine blue and inspected under a Nikon Ti Microscope.

For scanning microscopy, mature kernels were cut along their longitudinal axis to obtain the maximum longitudinal section, and the samples were dried to a critical point using a dryer (LEICA EM CPD); the dried samples were mounted on the surface of a brass disc using double-sided adhesive silver tape, coated with gold/palladium by a sputter-coating unit (EIKO IB-3), and scoped by a scanning electron microscope S-3400N (Hitachi, Tokyo, Japan).

Map-based cloning

Thirty kernels (pericarp removed) each with the WT *Dek701* or *dek701* mutant phenotype were collected from the same F_2 ear at 16 DAP for BSR-seq analysis. Total RNA was extracted from embryo and endosperm using an RNA extraction kit (Tiangen, Beijing, China). Complementary DNA (cDNA) libraries were constructed using an Illumina RNA-sequencing (RNA-Seq) sample preparation kit, and sequenced using an Illumina Hiseq2500 instrument (www.illumina.com). The sequencing data were trimmed and aligned to the B73 reference genome (B73 RefGen_v3) using HISAT2 (v.2.1.0). Only reads that mapped uniquely to the genome were retained for single nucleotide polymorphism (SNP) calling. Linkage analysis between SNPs and the target gene was performed following the parameters previously described (33).

Fine-mapping was conducted using 11520 homozygous mutant kernels from F_2 populations derived from the crosses *dek701* × B73 and *dek701* × Zheng58. The molecular markers developed for fine-mapping are listed in Supplemental Data Set S1.

RNA extraction, RT-PCR and RT-qPCR

Plant tissues were frozen in liquid nitrogen and ground to powder with a mortar. Total RNA was extracted using the RNAprep pure plant kit (TianGen, Beijing, China) and treated with RNase-free DNase I to remove DNA contaminants (Takara, Shiga, Japan). RT was conducted with TransScript II reverse transcriptase (Transgen Biotech, Beijing, China). RT-PCR was performed using the primers listed in Supplemental Data Set S1.

qPCR was performed using the TranStart Green qPCR SuperMix (Transgen Biotech) on a 7300 Real-time PCR system (Applied Biosystems, Waltham, MA). The $2^{-\Delta\Delta Ct}$ method was employed to calculate relative gene expression levels, using maize *GAPDH* (GRMZM2G046804) as internal control. The primers used are listed in Supplemental Data Set S1.

Vector construction for maize transformation

The sgRNA sequence were designed in the third exon of *Dek701* using CRISPR-P web base resource (http://crispr.hzau.edu.cn/CRISPR2/) (34), and 20 bp sgRNA sequence (CTACTGCTGCAGGCGAATGC) was chosen. The PCR fragments amplified from pCBC-MT1T2 were inserted between the *Bsa*I sites of pBUE411 (35) to construct the pBUE411-Dek701 vector. For molecular complementation of the *dek701* mutant, the *Dek701* coding sequence was cloned into pCAMBIA3301 to generate the overexpression vector *35Spro:RPABC5*. *Agrobacterium tumefaciens* strain LBA4404 containing the constructs were used to transform maize inbred line CAL or Z31 (36).

Subcellular localization of DEK701

The *Dek701* coding sequence was cloned into the pEarleyGate101 and pEarleyGate104 expression vectors to generate *Dek701-YFP* and *YFP- Dek701* fusion vectors, respectively, using LR-mediated Gateway recombination (Invitrogen, Carlsbad, CA). The fusion constructs were introduced into maize protoplasts using the polyethylene glycol/calcium-mediated transformation method (37). The fusion proteins were observed using a Zeiss LSM700 fluorescence microscope (Zeiss, Jena, Germany) after an incubation of 24 h in the dark. The fusion constructs were also transformed into Agrobacterium strain GV3101 and infiltrated into *N. benthamiana* leaves together with a construct encoding the nuclear protein marker AtHOOK fused to red fluorescent protein. The fluorescence signals were monitored under a Zeiss LSM700 confocal microscope after a 48-h incubation.

Yeast one-hybrid (Y1H) assay

The *Opaque2* coding sequence was cloned into the pB42AD vector (Clontech, Mountain View, CA) and co-transformed with a modified pLacZ vector (38) that contained the *LacZ* reporter driven by the promoter region of *ZmRPABC5a* or *Dek701* in the yeast strain EGY48. The transformants were grown on synthetic defined (SD) medium lacking uracil and tryptophan (SD −Ura −Trp) and containing 5-bromo-4-chloro-3-indolyl-β-d-galactopyranoside for blue color development.

Yeast two-hybrid (Y2H) assay

pDEST22-AD and pDEST32-BD constructs were generated by cloning the coding sequences of *Dek701* and other RNAP subunit genes. Appropriate pairs of constructs were co-transformed into yeast strain MaV203. Positive colonies were first selected on SD medium lacking leucine and tryptophan (SD –Leu –Trp) and then restreaked onto a SD –Leu –Trp –His –Ade medium containing 3-amino-1,2,4-triazole as a competitive inhibitor of the product of the *HIS3* gene, and 5-bromo-4-chloro-3-indolyl-α-d-galactopyranoside for blue color development. Primers used for cloning the coding sequences are listed in Supplemental Data Set S1.

Luciferase complementation image (LCI) and bimolecular fluorescence complementation (BiFC) assays

The coding sequences of *Dek701* and *ZmRPABC2* were cloned into pCAMBIA-nLUC and pCAMBIA-cLUC constructs, respectively. The LCI assay was performed in *N. benthamiana* leaves by Agrobacterium-mediated infiltration (39,40). Two days after infiltration, Luciferin (100 mM) was spread on the back of leaves for 15 min under dark condition, and luciferase activity was analyzed using a LB985 NightSHADE (Berthold Technologies, Bad Wildbad, Germany).

BiFC was performed in *N. benthamiana* leaves according to a previous work (41). The coding sequences of *Dek701* and *ZmRPABC2* were individually cloned into the pEarleygate201 and pEarleygate202 vectors harboring the nYFP and cYFP sequences, respectively, and co-infiltrated into *N. benthamiana* leaves through Agrobacterium-mediated transient infiltration. YFP fluorescence was detected after 48 h using a Zeiss LSM700 fluorescence microscope. Primers used for cloning of LCI and BiFC constructs are listed in Supplemental Data Set S1.

RNA-seq analysis

Total RNA was extracted from WT and *dek701* kernels (seed coat removed) as three replicates using the RNAprep pure plant kit (TianGen). Sequencing libraries were generated according to the Illumina standard protocol. These libraries were sequenced on an Illumina NovaSeq platform by BerryGenomics Corporation (BerryGenomics, Beijing, China), as 150-bp paired-end reads. Clean reads were obtained through processing with Perl scripts, followed by aligning to the maize B73 genome (RefGen_V3) using TopHat (version: 2.0.12) (42). Estimations of gene expression levels were expressed as fragments per kilobase of transcript sequence per millions base pairs sequenced (43). Cufflinks (version: 2.2.1) (44) was employed to assemble the transcripts and tests for differential expression across RNA-seq samples. Corrected P value $\leq$0.05 and fold change $>$2 were set as the threshold for significant DEGs. The RNA-seq data are available from the National Center for Biotechnology Information Gene Expression Omnibus (www.ncbi.nlm.nih.gov/geo) under the series entry PRJNA792688.

For the differential analyses of lncRNAs in the RNA-seq data sets of WT and *dek701*, all lncRNA loci identified by Li (45) in the maize genome were included for estimating their expression levels and conducting differential expression tests first with Cufflinks. Significant DELs were then identified with the same settings as DEGs above (corrected P value $\leq$ 0.05 and fold change $>$ 2).

Electrophoretic mobility shift assay (EMSA)

The *Opaque2* coding sequence was cloned into the *Bam*HI and *Not*I sites of the vector pET-32a+ . The resulting construct was transformed into *Escherichia coli* BL21 cells, which were grown at 37°C in LB medium, and induced by the addition of isopropyl β-D-1-thiogalactopyranoside to a final concentration of 1 mM when the optical density at 600 nm was 0.6. The cells were harvested for purification of recombinant 6× His-Opaque2 fusion protein with Ni-NTA agarose (QIAGEN, Dusseldorf, Germany) and used for EMSA. Oligonucleotide probes (Supplemental Data Set S1) were synthesized and labeled according to the standard protocol from Invitrogen Technology (Invitrogen, Carlsbad, CA). Standard reaction mixtures for EMSA were treated and observed as reported previously (46). Biotin-labeled DNA was detected using the LightShift Chemiluminescent EMSA kit (ThermoFisher, Waltham, MA).

Transient expression assay

The full-length open reading frame (ORF) of *Opaque2* were cloned into the effector vector pGreen II 62-SK under the control of the CaMV 35S promoter. The promoter fragment of *Dek701* (2.1 kb upstream of ATG) was cloned into the reporter vector pGreen II 0800-LUC. CaMV35S promoter-driven REN was used as an internal control. Individual combinations of effector and reporter vectors were co-transformed into *Agrobacterium* strain GV3101 (pSoup-p19) cells, and the transformed *Agrobacterium* strains were used for the infiltration of young *N. benthamiana* leaves. After 3 d of incubation, firefly and Renilla luciferase signals were assayed using a Dual Luciferase Reporter Assay Kit (Vazyme, Nanjing, China).

Flow cytometry

Five WT or *dek701* mutant kernels were collected from the same ear. Three ear replicates were used. Flow cytometry was performed as previously described (47). A total of 15000 particles were collected and analyzed using Flowjo software (FlowJo, Ashland, OR).

Phylogeny and comparative genome analysis

The protein and coding sequences of *RPABC5* genes from different species were collected from Phytozome (https://phytozome-next.jgi.doe.gov/). The protein sequences were aligned with MUSCLE and converted into the corresponding codon alignment using PAL2NAL. Poorly aligned sequences were then removed by GBLOCKS. A neighbor-joining phylogenetic tree was constructed by MEGA software using 1000 bootstrap replicates.

Location of the rice WGD (inner-species collinearity) was extracted from the rice genome annotation project (http://rice.uga.edu) (48). Macro-collinearity across cereal genomes over the *RPABC5* and *RPABC2* genomic regions was extracted from www.gramene.org (49).

The Hapmap3 SNPs located in the gene and the flanking 5-kb regions were used to estimate the nucleotide diversity (π) of teosinte and maize lines. Nucleotide diversity was calculated by Vcftools in sliding window mode (window size = 1000 bp; step size = 100 bp). The selection pressure of domestication was measured as the ratio between π values from teosinte and maize. The loss of genetic diversity observed within maize was explained by the bottleneck of maize domestication; coalescent simulations following the demographic history of maize domestication inferred by (50) were performed by Hudson's Ms program, with parameters assigned as previously described (51,52), and 10 000 coalescent simulations were performed. The observed values that deviated significantly from expectations under the

neutral domestication of maize indicate selection in the examined region.

Expression genome-wide association study of the *dek701* gene

An association population consisting of 368 maize inbred lines which was previously genotyped and characterized (53–55) was used for expression genome-wide association study. Transcriptomic sequencing was previously conducted on the immature kernels at 15 DAP of these inbred lines and was quantified for the *Dek701* gene (54). Using 296 5911 SNPs with MAF ≥0.05 of the 368 inbred lines, the association analyses between SNPs and gene expression were performed using a linear mixed model implemented in TASSEL v5 (TASSEL). The population structure was used as covariates, and the kinship matrix was used as the variance-covariance matrix of the random effects (54). The threshold for significance was set as $P = 1 \times 10^{-6}$.

RESULTS

The *dek701* mutant displays delayed endosperm development

dek701 is a spontaneous mutant isolated after multiple rounds of self-pollination from the progeny of a hybrid plant, which was derived from a cross between inbred lines Chang7-2 and G38. Compared to kernels homozygous for the *Dek701* allele and used as wild type (WT), mature *dek701* kernels were smaller and varied in size (Figure 1A and B). The 100-kernel weight of the *dek701* mutant was 48.8% that of the WT (Figure 1C). We crossed *dek701* to inbred lines B73, Z58, Chang7-2 and Mo17 to generate segregating populations, with which we determined that WT and *dek* kernels in F_2 ears follow a 3:1 segregation ratio ($\chi^2 = 0.27–2.02 < \chi^2_{0.05} = 3.84$) (Supplemental Figure S1A and B), indicating that *dek701* is a monogenic and recessive mutation.

We observed that both mature *dek701* endosperm and embryo are smaller in size than those of the WT (Figure 1D). At 21 days after pollination (DAP), both *dek701* and WT embryos had formed the scutellum, a leaf primordium, a shoot apical meristem (SAM) and a root apical meristem (RAM) (Figure 1E). Compared to WT kernels with a starch-filled endosperm, *dek701* kernels displayed a small endosperm, with a gap observed between the endosperm and the pericarp at 21 DAP (Figure 1E; Supplemental Figure S2). These results indicate that endosperm development were abnormal in *dek701*, whereas *dek701* embryos retained the ability to form typical embryonic structures. The germination rate of *dek701* seeds decreased to 68.6%, compared to the germination rate of 98.2% seen for the WT (Figure 1F and G). Although germinated *dek701* seedlings grew poorly in the early growth stage (Supplemental Figure S3A and B), adult *dek701* plants showed plant height, total leaf number and anthesis time similar to those of WT sibling plants at the flowering stage (Figure 1H and I; Supplemental Figure S3C–F). After self-pollination, *dek701* also produced a cob of similar size as the WT, as well as *dek* kernels with a clearly visible embryo but underdeveloped endosperm characteristic of this class of maize mutants (Figure 1H; Supplemental Figure S3G). *dek701* embryos were harvested at 16 DAP and allowed to grow on Murashige and Skoog medium for 6 d, resulting in a similar germination rate as that seen with WT sibling embryos (Figure 1J and K), indicating that *dek701* embryos retained full germination capacity. However, these rescued *dek701* seedlings showed weak growth compared to the WT (Supplemental Figure S3H and I). These results suggest that the loss of *Dek701* function did not affect the function of embryos in the pre-embryo stage.

We also investigated endosperm structure using scanning electron microscopy (SEM). Whereas WT endosperm was filled with smooth and spherical starch granules (SGs), the *dek701* endosperm was loosely packed by irregularly shaped SGs in the center of the endosperm (Supplemental Figure S4A). When starch and protein contents were reflected as percentage of kernel weight, the total starch content of *dek701* endosperm was lower by 12.2% relative to the WT (Supplemental Figure S4B); total protein, zein protein and nonzein protein contents in *dek701* endosperm were higher than those of the WT (Supplemental Figure S4C), and among zein proteins, the contents of 19, 22 and 27-kDa zein proteins visibly increased in *dek701* endosperm (Supplemental Figure S4D and E). However, when starch and protein contents were reflected as the average contents per kernel, the starch and protein contents of the *dek701* endosperm were significantly lower than those of the WT endosperm (Supplemental Figure S4F and G).

Positional cloning of *Dek701*

To identify *Dek701*, we performed bulked segregant RNA-Seq (BSR-Seq) using *dek* and WT kernels from segregating F_2 ears derived from a *dek701* × B73 cross. We mapped the *Dek701* locus to a 3.09-Mb interval on chromosome 8 (Supplemental Figure S5). We developed additional markers within this interval (Supplemental Data Set S1), which narrowed down the location of the candidate gene to a 22-kb region using 11520 individual *dek* kernels. This final region contained four annotated genes in the B73 reference genome (RefGen V3): GRMZM2G316214, GRMZM5G834335, GRMZM2G020583 and GRMZM2G020594 (Figure 2A). Transcripts for GRMZM2G316214 and GRMZM2G020583 were undetectable in either *dek701* or WT kernels in our RNA-seq dataset. GRMZM2G020594 exhibited similar expression levels in WT and *dek701*, while the expression of GRMZM5G834335 was lower in *dek701* compared to WT (Supplemental Data Set S2), indicating that GRMZM5G834335 might be *Dek701*.

We attempted to amplify and sequence the genomic region encompassing GRMZM5G834335 from WT and *dek701*, but failed to obtain a PCR product for the 5′ untranslated region of GRMZM5G834335 in *dek701*. We thus applied several rounds of thermal asymmetric interlaced PCR, culminating in the identification of a large fragment replacement (Supplemental Data Set S3) from –4130 bp to + 113 bp relative to the ATG of GRMZM5G834335 in *dek701* (Figure 2B), which only caused the defect of GRMZM5G834335 gene, but not affected the structure and expression of other three nearby genes. In addition, reverse

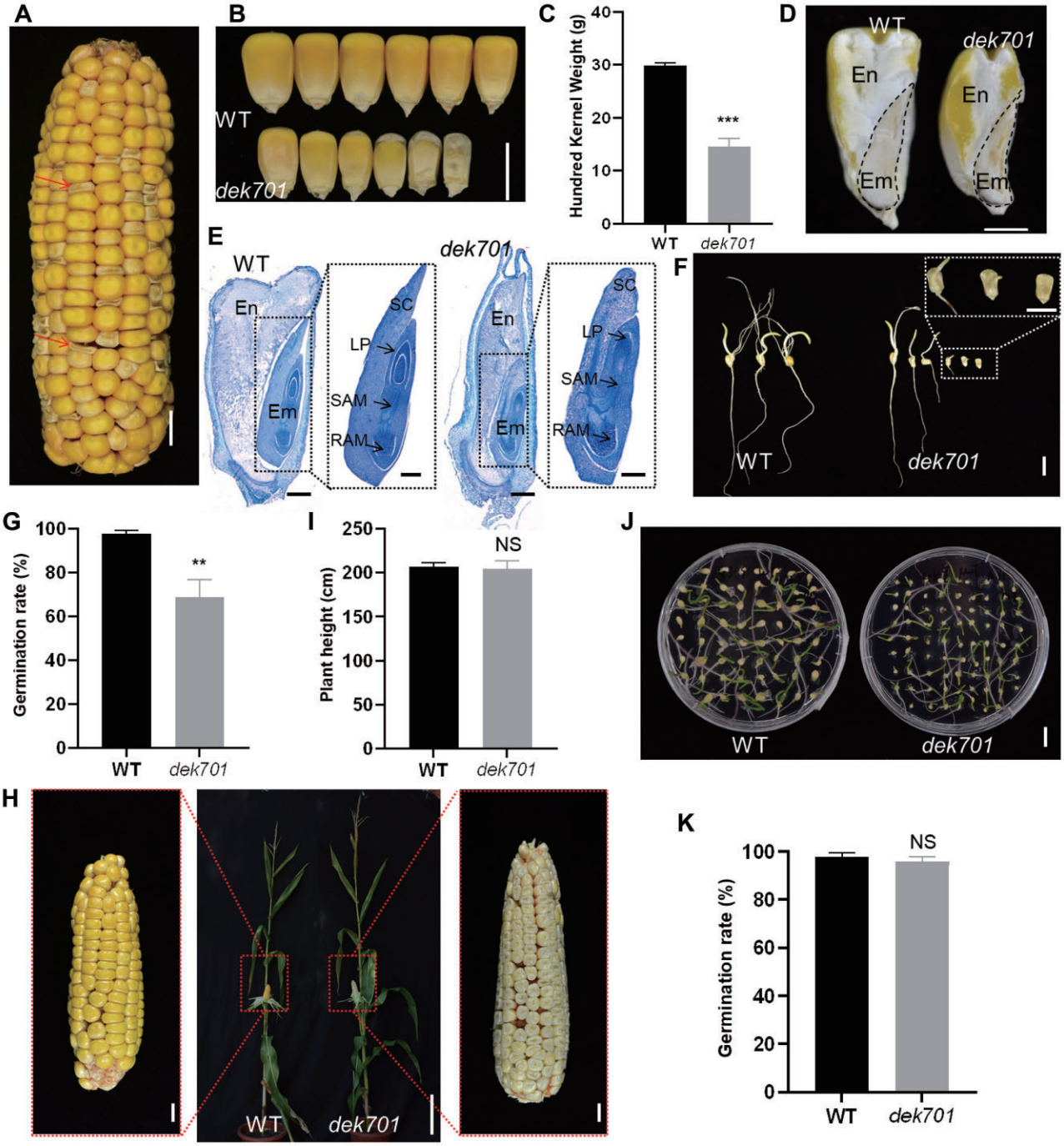

Figure 1. Phenotypic characterization of kernels from the *dek701* mutant. (**A**) A mature self-pollinated heterozygous *dek701* ear. Red arrows indicate *dek701* kernels. Bar = 1 cm. (**B**) Mature *dek701* kernels and wild-type (WT) siblings from a mature self-pollinated heterozygous *dek701* ear. Scale bar = 1 cm. (**C**) Mean 100-kernel weight calculated from (B). Values are means ± standard deviation (SD, $n = 3$; ***$P < 0.001$ as determined by Student's *t*-test). (**D**) Longitudinal sections of mature *dek701* kernel and WT sibling. En, endosperm; Em, embryo. Scale bar = 2.5 mm. **(E)** Longitudinal paraffin sections of WT sibling and *dek701* kernel at 21 DAP. SC, scutellum; LP, leaf primordia; SAM, shoot apical meristem; RAM, root apical meristem. Scale bars = 1 mm (0.5 mm in magnified picture). (**F**) Germination performance of WT siblings and *dek701* mature kernels. Picture was taken 5 d after seed hydration. Scale bar = 2 cm (1 cm in magnified picture). (**G**) Germination rate calculated from (F). Values are means ± SD ($n = 3$; ***$P < 0.001$ as determined by Student's *t*-test). (**H**) Representative mature *dek701* plant and WT sibling. Scale bar = 30 cm (1 cm in magnified picture). (**I**) Mean plant height calculated from (H). Values are means ± SD (n = 10; NS, no significant difference at $P < 0.05$ as determined by Student's *t*-test). (**J**) Germination performance of WT siblings and *dek701* embryos harvested at 16 DAP on half-strength Murashige and Skoog medium for 6 days. (**K**) Mean germination rates calculated from (J). Values are means ± SD ($n = 3$; NS, no significant difference at $P < 0.05$ as determined by Student's *t*-test).

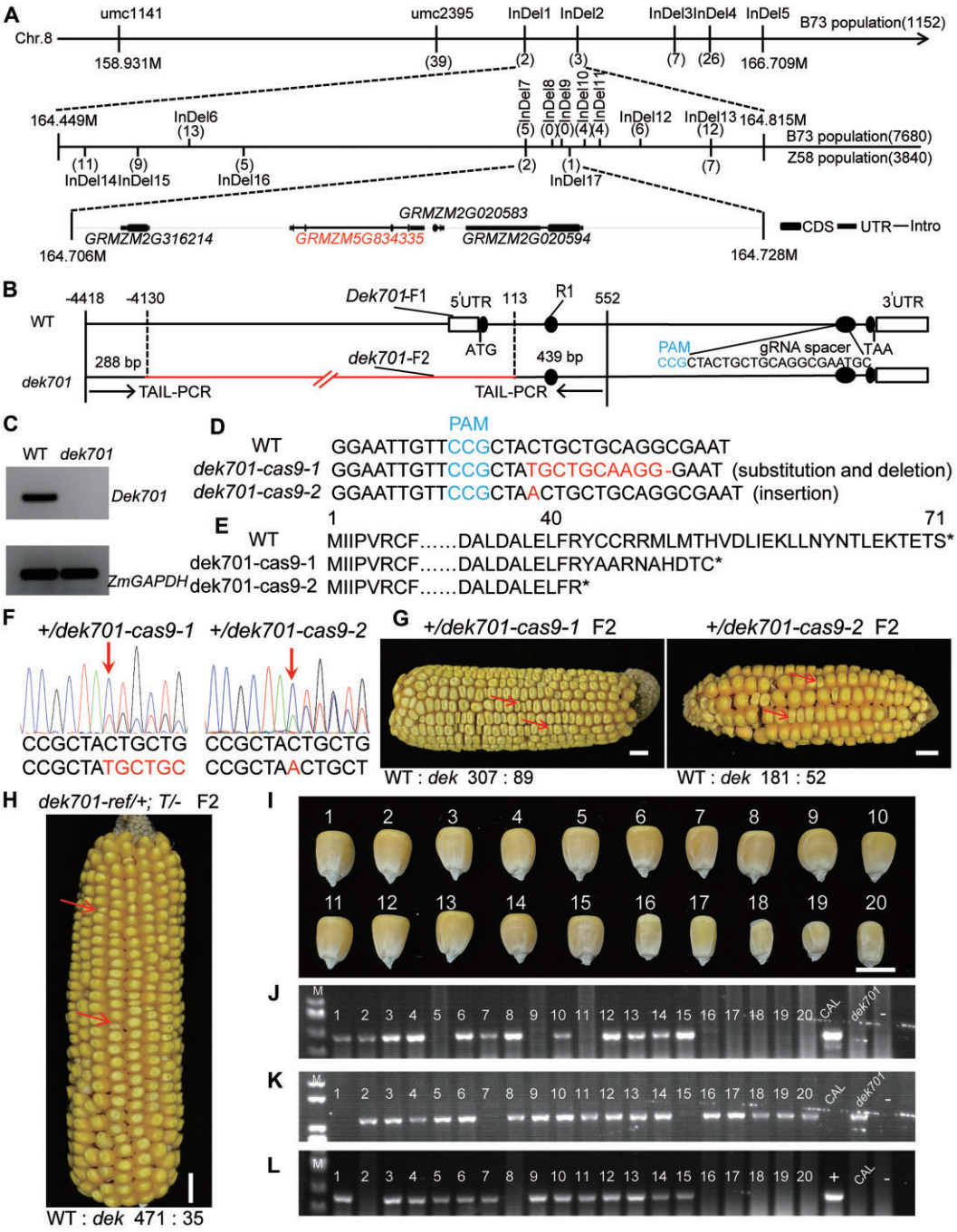

Figure 2. Positional cloning and identification of *Dek701*. (**A**) The *dek701* mutant was crossed to B73 and Z58 inbred lines to generate F_2 ears. The numbers in parentheses below each molecular marker indicates the number of recombinant kernels identified from the 11520 investigated kernels. The *Dek701* locus was narrowed down to a 22-kb interval (from 164 706 812 bp to 164 728 730 bp) on chromosome 8, which contained four candidate genes. (**B**) Structure of the GRMZM5G834335 locus and position of *dek701* alleles. Lines, introns; black ellipses, exons; white rectangles, untranslated regions. The gRNA target sequence and the protospacer-adjacent motif (PAM) in the GRMZM5G834335 gene region for CRISPR/Cas9 editing are shown. *Dek701*-F1, *dek701*-F2 and R1 represent the primer sites. (**C**) RT-PCR analysis of *Dek701* expression in WT sibling and *dek701* kernels from the self-pollinated heterozygous *dek701* ear at 16 DAP. (**D**) The mutation of *Dek701* in two independent CRISPR-Cas9 mutants. Red letters and dashes represent insertions and deletions, respectively. (**E**) The deduced partial amino acid sequence of DEK701 from *dek701-cas9* plants. (**F**) Sequence peaks of heterozygous *dek701-cas9-1* and *dek701-cas9-2* at target site. Red arrows indicate the editing sites. (**G**) Mature self-pollinated heterozygous ears of *dek701-cas9-1* (Z31 background) and *dek701-cas9-2* (CAL background). Arrows indicate the mutant kernels. Bars = 1 cm. (**H**) F_2 ear produced from a cross between a transgenic event (T/–) and a *dek701* heterozygous plant (*dek701*/*Dek701*). Red arrows indicate *dek701* mutant kernels. (**I**) Representative kernels with the WT (1 to 15) and mutant (16 to 20) phenotype from (H). (**J**) WT sequence at *dek701* locus was identified in the kernels from (I) by PCR using primers *Dek701*-F1 and R1, which are indicated in (B). CAL, the maize inbred line used for transformation. *dek701*, homozygous *dek701*; –, water. (**K**) mutant sequence at *dek701* locus was identified in the kernels from (I) by PCR using primers *dek701*-F2 and R1, which are indicated in (B). CAL, the maize inbred line used for transformation. *dek701*, homozygous *dek701*; –, water. (**L**) PCR detection of the transgene in the kernels from (I) using primers (T-F/T-R) specific for the transgene. +, plasmid; –, water.

transcription PCR (RT-PCR) analysis showed that GRMZM5G834335 transcripts are not detected in *dek701* kernels (Figure 2C). Altogether, these results indicated that GRMZM5G834335 is a strong candidate for the causal locus *Dek701*.

Allelism and complementation test of *dek701*

To confirm the identity of *Dek701* as GRMZM5G834335, targeted mutation of GRMZM5G834335 was performed using the CRISPR/Cas9 system. The guide RNA (gRNA) spacer sequences were designed to target the third exon of GRMZM5G834335 (Figure 2B). The constructed plasmid was transformed into maize inbred lines Z31 or CAL, and two independent CRISPR/Cas9 transgenic lines (*dek701-cas9-1*, Z31 background; *dek701-cas9-2*, CAL background) were obtained that contained a substitution or insertion at the target sequence (Figure 2D and F), resulting in early termination of GRMZM5G834335 protein translation (Figure 2E). The F_2 ears generated by self-crossing of +/*dek701-cas9-1* or +/*dek701-cas9-2* plants displayed a 3:1 (307 : 89, $\chi^2 = 1.21$; 181 : 52, $\chi^2 = 0.76 < \chi^2_{0.05} = 3.84$) segregation of WT and mutant kernels (Figure 2G). Allelism tests were performed by crossing heterozygous *dek701* with heterozygous *dek701-cas9-1* and *dek701-cas9-2*, respectively. The F_1 ears displayed a 3:1 (281 : 97, $\chi^2 = 0.06$; 256 : 73, $\chi^2 = 1.24$) segregation of WT and *dek* kernels (Supplemental Figure S6A), and the randomly selected *dek* kernels contained both the *dek701* locus and the *dek701-cas9* locus (Supplemental Figure S6B to D). These results demonstrate that *dek701-cas9* mutants and *dek701* mutant cannot rescue the *dek* phenotype one another, supporting that GRMZM5G834335 is *Dek701*.

As an independent confirmation that GRMZM5G834335 is *Dek701*, we amplified the coding region from inbred line B73 and placed it under the control of the cauliflower mosaic virus 35S promoter. We introduced the resulting construct into inbred line CAL and identified transgenic events with a single-copy insertion through identifying 3:1 segregation of transgene in T_2 generation (Supplemental Figure S7A). We obtained three independent transgenic events that were then crossed to *dek701*/*Dek701* plants to generate heterozygous F_1 plants. The individual F_1 plants with heterozygous *dek701*/+ genotype and hemizygous for the transgenic locus were identified and self-crossed to obtain F_2 ears. As expected in the case of complementation, all the F_2 ears exhibited a phenotypic segregation ratio of 15:1 between WT and *dek701* mutant kernels (Figure 2H; Supplemental Figure S7B and C). Furthermore, we genotyped kernels from the F_2 population of event 1 with specific primers to identify *dek701* locus (Figure 2J and K), followed by genotyping to detect the presence of the *35Spro:Dek701* transgene (Figure 2L). We determined that all homozygous *dek701* kernels carrying the transgene showed a WT phenotype, whereas kernels lacking the transgene retained the mutant phenotype (Figure 2I). Altogether, Allelism test and transgenic rescue assays demonstrated that GRMZM5G834335 is the causative gene for *Dek701*.

Dek701 encodes the common RNA polymerase subunit RPABC5b

Dek701 was predicted to encode the RNA Pol common subunit RPABC5, comprising 71 amino acids. The genome for each of six typical seed plants selected harbored two *RPABC5* copies: the gymnosperm Norway spruce (*Picea abies*), the dicot angiosperms Arabidopsis and black cottonwood (*Populus trichocarpa*), and the monocot angiosperms purple false brome (*Brachypodium distachyon*), rice, sorghum (*Sorghum bicolor*) and maize. By contrast, we identified a single copy in the green alga *Chlamydomonas reinhardtii*, the bryophyte *Physcomitrium patens*, and the pteridophyte *Selaginella moellendorffii* (Figure 3A).

The short protein length made it difficult to unambiguously assign phylogenetic relationships among RPABC5 homologs, prompting us to perform a synteny analysis (comparative genome analysis) focusing on *RBABC5* genes from the Poaceae, since Poaceae species evolved from a common ancestor 50–70 million years ago (mya) (56). Cross-species comparisons at the micro-collinearity level showed that GRMZM5G803992 is located on collinear chromosomal regions in *B. distachyon* (containing the ortholog Bradi4g41090), rice (containing the ortholog Os12g07980), and sorghum (with the ortholog Sobic.008G058300), suggesting that these four orthologs evolved from a common ancestor before the split of Poaceae species (Figure 3B). Thus, we named these evolutionarily conserved orthologs *RPABC5a* and the others (including *Dek701*) *RPABC5b*.

A whole-genome duplication (WGD) was predicted to have occurred in the common rice ancestor about 70 mya (48). Rice and sorghum *RPABC5b* mapped to chromosomal regions sharing micro-collinearity over the *RPABC5a* regions (Figure 3B), indicating that rice and sorghum *RPABC5a* and *RPABC5b* are the result of the WGD in the cereal ancestor. However, maize *ZmRPABC5a* and *Dek701* (*ZmRPABC5b*) mapped to different chromosomes, indicating that *Dek701* was duplicated via an intrachromosomal duplication of a maize chromosome, probably by unlinked (transposed) duplication, rather than by linked (tandem) duplication (57). RT–quantitative PCR (RT-qPCR) analysis revealed that *Dek701* is constitutively expressed in a broad range of maize tissues, including stems, roots, leaves, bracts, tassels, silk, embryos and endosperm, with relatively high expression levels in kernels, especially in the endosperm (Figure 3C). During kernel development, *ZmRPABC5a* and *Dek701* expression increased gradually from 12 DAP to 24 DAP and decreased slightly at 30 DAP (Figure 3D).

To examine the subcellular localization of DEK701, we generated constructs encoding a fusion between full-length DEK701 and the N or C terminus of the yellow fluorescent protein (YFP). We transiently expressed the resulting constructs in both maize protoplasts and *Nicotiana benthamiana* leaf epidermal cells; we observed YFP fluorescence in the nucleus and the cytoplasm (Figure 3E and F), indicating that DEK701 accumulates in the nucleus and the cytoplasm.

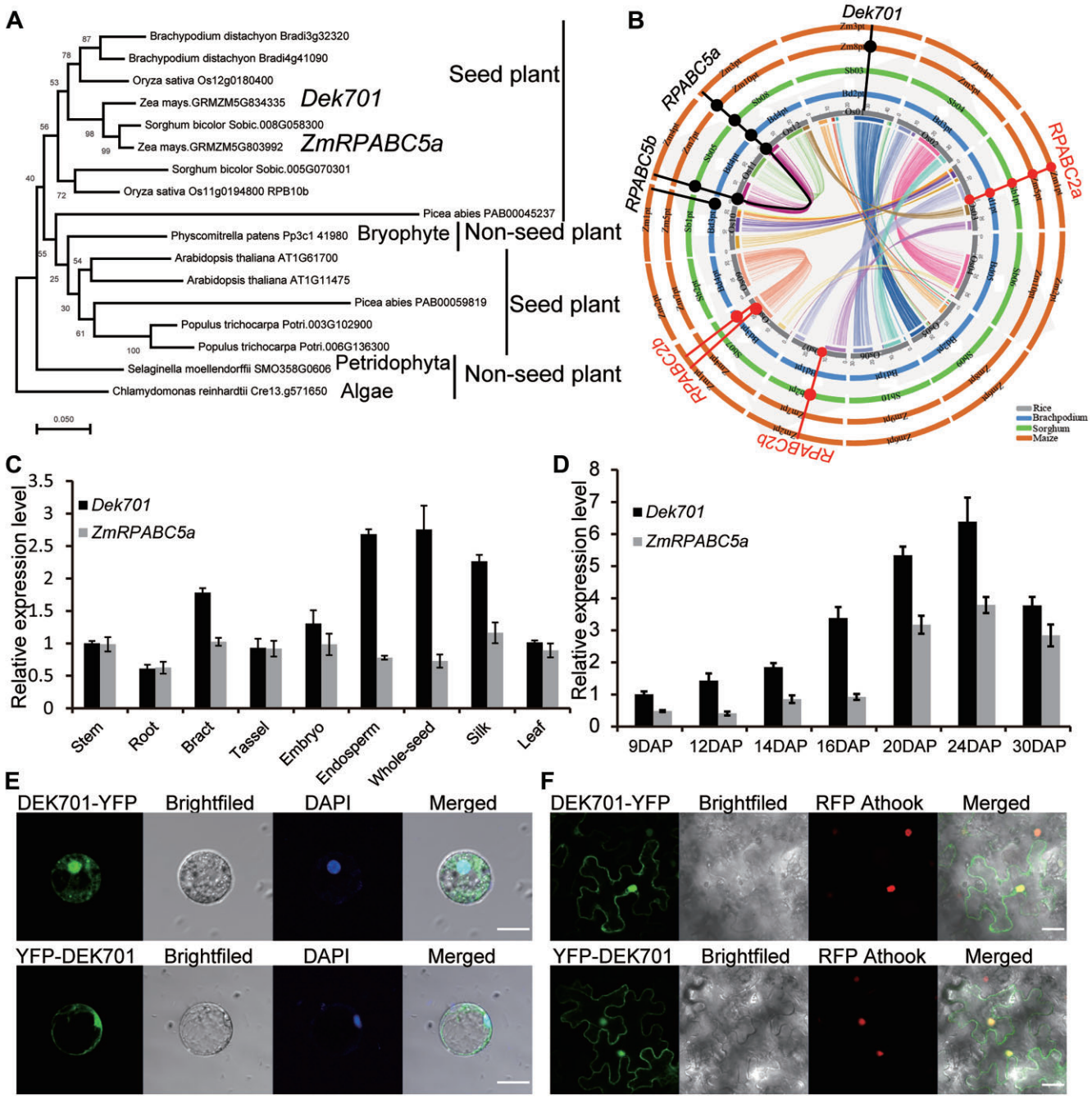

Figure 3. Phylogenetic analysis, expression pattern of *Dek701*, and subcellular localization of DEK701. (A, B) Phylogenetic tree of plant RPABC5 proteins. RPABC5-like proteins were identified by BLASTP searches at Phytozome. (**A**) Phylogenetic tree of *RPABC5* genes based on DNA sequence alignment with ClustalW using the neighbor-joining method with 1000 bootstrap replicates. (**B**) Collinearity analysis of *ZmRPABC5* genes in rice, *B. distachyon*, sorghum and maize. (C, D) RT-qPCR analysis of relative transcript levels of *Dek701* and *ZmRPABC5a* in major maize tissues (**C**) and in kernels at different DAP (**D**). Stem, root, bract, leaf, silk, and tassel tissues were collected from B73 plants at the flowering stage. The whole seed, endosperm, embryo in (C) was harvested at 12 DAP. *ZmGAPDH* was used as internal reference. Values are means ± SD of three biological replicates. (E, F) Subcellular localization of the DEK701-YFP fusion in maize leaf protoplasts (**E**) and *N. benthamiana* leaf epidermal cells (**F**). YFP, yellow fluorescence protein; DAPI, 4,6-diamidino-2-phenylindole staining to reveal nuclei; Athook, a nuclear marker; RFP, red fluorescent protein.

Dek701 expression is transcriptionally regulated by Opaque2

During kernel development, *Dek701* and *ZmRPABC5a* showed similar expression patterns, however, *Dek701* had specifically higher expression level in endosperm and was always expressed at a higher level than *ZmRPABC5a* (Figure 3C and D). To dissect the expression regulation, we investigated the expression quantitative trait loci (eQTLs) that associated with the expression of *Dek701* using the published data from 368 maize lines (54), and a *cis*-eQTL was found in the promoter region of *Dek701* (Figure 4A). We therefore analyzed the *Dek701* and *ZmRPABC5a* promoter sequences at the PlantCARE website (https://bioinformatics.psb.ugent.be/webtools/plantcare) and identified a GCN4 (general control nondepressible4) motif specifically in the *Dek701* promoter that is a known target site for the key endosperm developmental regulator Opaque2 (58,59) (Supplemental Figure S8). We confirmed that Opaque2 can bind to the promoter of *Dek701*, but not that of *ZmRPABC5a*, in a yeast one-hybrid (Y1H) assay (Figure 4B). To further confirm the binding of Opaque2 to *cis*-elements in the *Dek701* promoter, we performed electrophoretic mobility shift assays (EMSAs) with purified recombinant His-Opaque2 protein and a labeled 50-bp DNA probe containing the GCN4 motif from the *Dek701* promoter. A probe that has been experimentally confirmed to the target of Opaque2 (46) was synthesized as a positive Opaque2 probe control, and a shift in mobility was detected (Figure 4C, lane 2). When recombinant His-Opaque2 protein was incubated with the labeled *Dek701* probe, a clear binding was also detected and this binding gradually decreased with increasing amount of unlabeled DNA (Figure 4C), supporting the notion that Opaque2 can directly bind to the *Dek701* promoter *in vitro*. Moreover, luciferase based transient transactivation assays verified that Opaque2 activates the expression of *Dek701* (Figure 4D).

We also investigated whether the loss of Opaque2 function affected *Dek701* expression. Relative *Dek701* transcript levels were about two-fold lower in the endosperm of the *o2* mutant compared to WT (W22 inbred line) but accumulated to comparable levels in WT and *o2* in other tissues (Figure 4E). We did not observe significant expression differences between WT and the *o2* mutant for *ZmRPABC5a*. These results indicate that the evolutionary gain of a GCN4 *cis*-element in the *Dek701* promoter may have contributed to its high expression in maize endosperm.

To assess whether *Dek701* was a target of selection during domestication, we analyzed nucleotide diversity around the *Dek701* locus using the third-generation *Zea mays* haplotype map (HapMap 3) (60). A sliding-window analysis revealed elevated DNA polymorphism rates between teosinte and maize lines over the *Dek701* promoter region (π teosinte/π maize = 4.25), indicative of a decrease in nucleotide diversity in modern maize compared to teosinte germplasm (Figure 4F and G). Coalescent simulations incorporated the demographic history of maize domestication and showed a significant ($P < 0.01$) deviation from the neutral expectation. These results indicate that the *Dek701* promoter region was subjected to strong artificial selection during the domestication of maize.

Loss of function of DEK701 affects function of RNA pols

As DEK701 is a common subunit of Pol I, II and III, we speculated that loss of DEK701 function might affect RNAP complex formation and transcription efficiency in *dek701* mutants. To reveal the effects associated with loss of DEK701 function on transcription, we performed an RNA-seq analysis using *dek701* and WT sibling kernels at 15 DAP. We identified 1565 upregulated and 930 downregulated differentially expressed genes (DEGs) in *dek701* relative to WT (Supplemental Data Set S2), of which 1736 DEGs were functionally annotated by Gene Ontology (GO) analysis (http://systemsbiology.cau.edu.cn/agriGOv2/). Notably, 488 DEGs were related to RNA biosynthesis, transcription regulator activity, and DNA binding, all GO terms that play important roles in transcription (Figure 5A; Supplemental Data Set S4). We also determined that 107 DEGs are associated with response to phytohormone stimulus (GO:0009725), of which 24 DEGs were related to auxin signaling, with 11 genes encoding repressors from the auxin/indole-3-acetic acid (IAA) family being upregulated (Figure 5B). In addition, nine DEGs were involved in abscisic acid (ABA) signaling, with five downregulated genes encoding ABA receptors PYR1/PYL/RCAR (PYRABACTIN RESISTANCE1/PYR-LIKE/ regulatory component of ABA receptor) and the positive ABA signaling component SnRK2 (Snf1-related protein kinase2), while four upregulated genes encoded negative regulators of ABA signaling from the protein phosphatase 2C (PP2C) family (Figure 5B). These results suggested that both auxin and ABA signaling pathways are repressed in *dek701*. GO terms associated with nutrient reservoir activity (GO:0045735) and carbohydrate metabolism (GO:0005975) were also enriched. Most of the genes related to these GO terms exhibited lower expression in *dek701* than in WT. For example, several genes participating in starch biosynthesis were downregulated, such as *Shrunken 1* (*Sh1*), *Sh2*, *Starch synthase I* (*SSI*) and *SSIIa* (Supplemental Data Set S4). 12 key genes (GO:0045735) involved in protein metabolism were also significantly downregulated in *dek701* (Supplemental Data Set S4). These results were consistent with the lower accumulation of nutrient reservoirs in *dek701* kernels.

We also investigated whether the transcription of long ncRNA (lncRNA) was affected in *dek701*, leading to the identification of 279 upregulated and 329 downregulated differentially expressed lncRNAs (DELs) in *dek701* compared to the WT (Figure 5C and Supplemental Data Set S5), indicating that loss of DEK701 function also influenced the transcription of lncRNA loci. We validated the expression levels of 33 randomly selected genes involved in RNA biosynthesis, phytohormone signal transduction, and starch biosynthesis, as well as 10 lncRNAs, by RT-qPCR analysis (Figure 5D and E).

As DEK701 is also a common subunit of Pol I and III, we investigated whether the transcription of rRNA and tRNA was altered in 15-DAP *dek701* kernels by RT-qPCR. We observed a marked decrease in the levels of the three rRNAs tested in *dek701* compared to WT, indicating that Pol III is also affected by the loss of DEK701 function (Figure 5F). Furthermore, we determined that riboso-

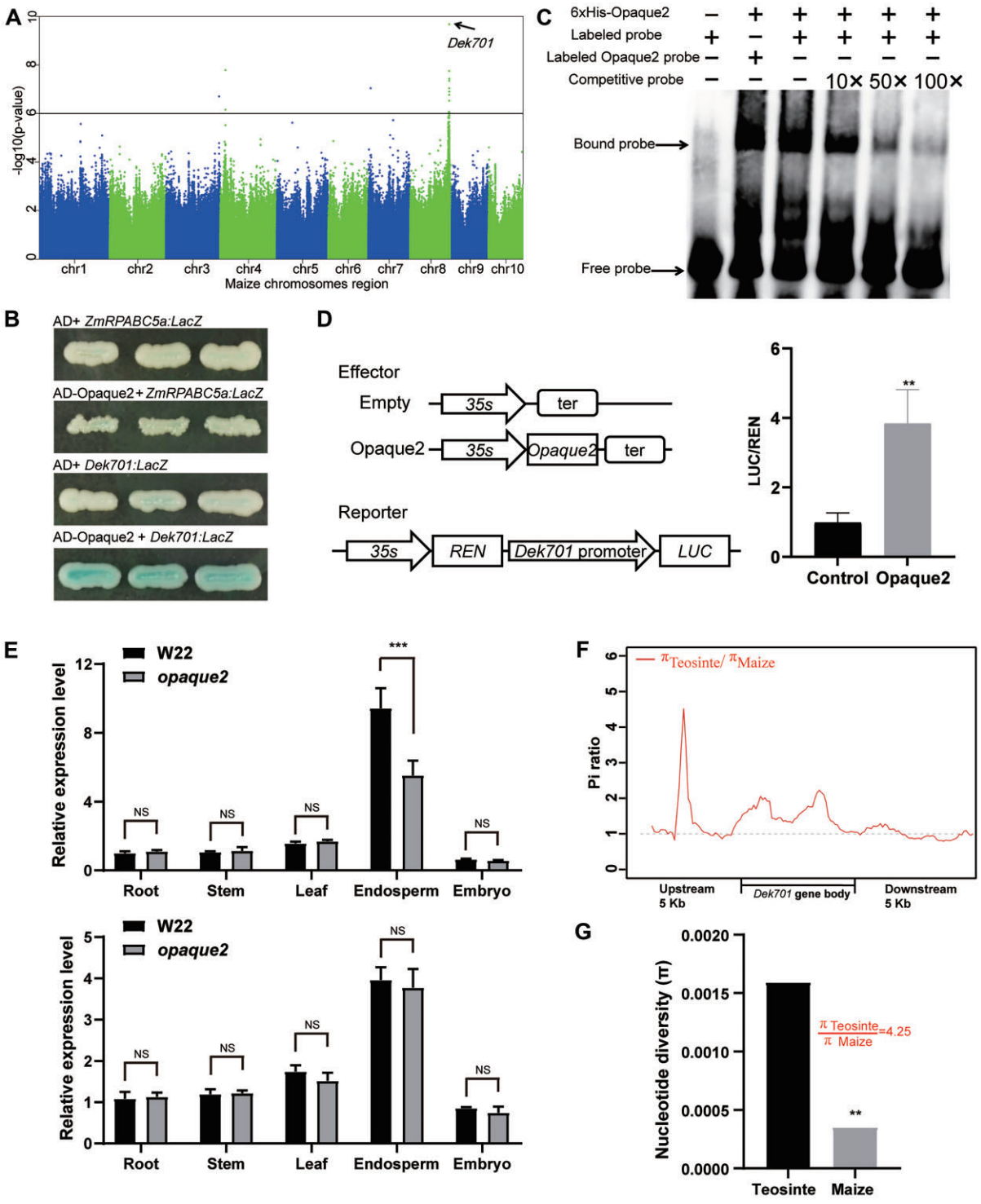

Figure 4. *Dek701* expression is transcriptionally regulated by Opaque2 (O2). (**A**) Genome-wide distribution of eQTLs for *Dek701* in developing maize kernels. (**B**) Y1H assay showing that Opaque2 directly binds to the *Dek701* promoter but does not bind to the *ZmRPABC5a* promoter. (**C**) EMSA with recombinant purified His-Opaque2 fusion protein and DNA probes. Labeled probe, GCN4 motif from the *Dek701* promoter; labeled Opaque2 probe, Opaque2 binding site from the promoter of an Opaque2 target gene GRMZM2G086294 (46). The probe sequences are listed in Supplemental Data Set S1. (**D**) Opaque2 activates the *Dek701* promoter in transient dual-luciferase transactivation assay. Left: plasmids for transactivation assay. Right: data are shown as relative ratios of the transcriptional activities conferred by Opaque2 expression to the empty vector control. LUC/REN, ratio of firefly luciferase to Renilla luciferase activity. Data are presented as means ± SD (n = 3). $^{**}P < 0.01$ (Student's *t*-test). (**E**) RT-qPCR analysis of *Dek701* (top) and *ZmRPABC5a* (bottom) expression in major maize tissues in WT (W22 inbred line) and *o2* (W22 background) plants. Values are means ± SD ($n = 3$; $^{***}P < 0.001$; NS, no significant difference as determined by Student's *t*-test). (**F**) Signature of artificial selection at the *Dek701* locus, as determined by the ratio between π values from teosinte and maize. (**G**) Resequencing analysis and coalescence simulations validating the 5′ regulatory region of *Dek701* as a target of selection. *P* values were determined using coalescence simulations: $^{**}P < 0.01$.

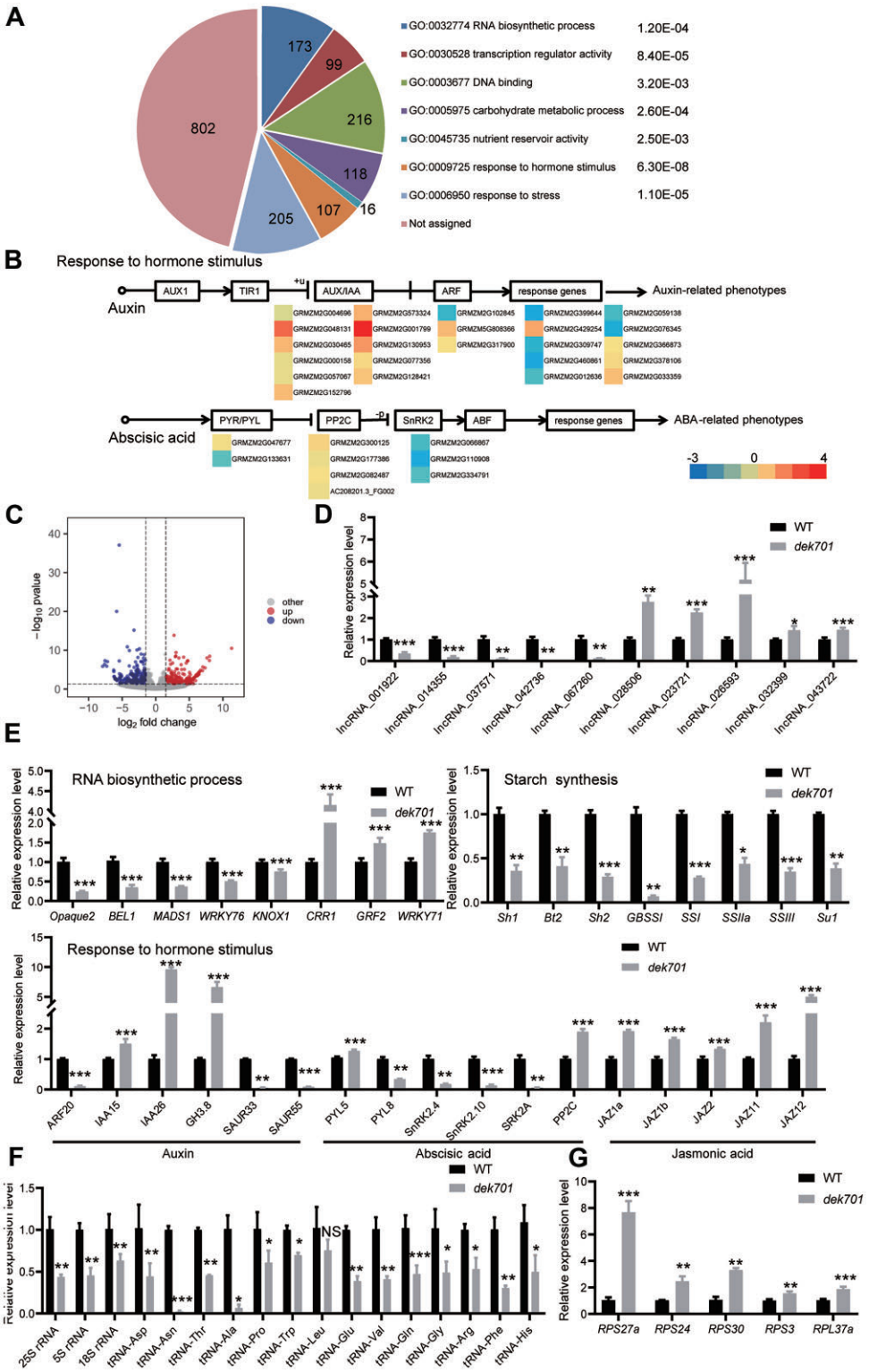

Figure 5. Transcriptome alterations in *dek701*. (**A**) Top most significantly enriched GO terms among DEGs between WT sibling and *dek701* mutant, based on RNA-seq analysis. The number of genes and the *P* value for each GO term are shown. E indicates 10 raised to the indicated power in scientific notation. (**B**) Identified DEGs involved in response to phytohormone stimulus. The signal transduction pathways are as previously described (61). The colored boxes to the left of the gene name represent upregulated (red) and downregulated (green) genes in *dek701* compared to WT sibling. (**C**) Number of DELs in the *dek701* endosperm compared to WT sibling. (**D**) RT-qPCR confirmation of 10 DELs in 16-DAP endosperm of WT sibling and *dek701*. (**E**) RT-qPCR confirmation of 33 representative DEGs associated with RNA biosynthesis, phytohormone response and starch biosynthesis. Values are means ± SD ($n = 3$; $^*P < 0.05$; $^{**}P < 0.01$; $^{***}P < 0.001$ as determined by Student's *t*-test). (**F**) RT-qPCR analysis of tRNA and rRNA genes in 16-DAP endosperm of WT sibling and *dek701*. (**G**) RT-qPCR analysis of ribosomal protein genes in 16-DAP endosperm of WT sibling and *dek701*. Values are means ± SD ($n = 3$; $^*P < 0.05$; $^{**}P < 0.01$; $^{***}P < 0.001$ as determined by Student's *t*-test). All transcript levels were normalized to *GAPDH*.

mal protein genes encoding small ribosomal subunits (*Rps*) and large subunits (*Rpl*) are expressed to higher levels in *dek701* kernels relative to WT, which might make up for the lower abundance of rRNAs through a compensatory mechanism (Figure 5G). Among the 17 tRNAs in the maize genome (18), we detected the expression of 14 tRNAs, 13 of which accumulated to lower levels in *dek701* compared to WT (Figure 5F), indicating impaired Pol I function in *dek701*.

Loss of function of DEK701 affects cell proliferation and phytohormone homeostasis

To explore how the loss of DEK701 function might cause the *dek* phenotype, we inspected cell morphology in developing *dek701* and WT sibling kernels. Compared to WT, *dek701* kernels were characterized by structurally irregular basal endosperm transfer layer cells with defective cell wall ingrowth (Figure 6A). However, embryo cells were uniformly arranged in both WT and *dek701* (Figure 6B), with similar cell number and cell size (Figure 6C and D). In WT endosperm, cells were regularly and closely arranged, whereas the *dek701* endosperm typically comprised cells that were arranged irregularly and loosely (Figure 6E). Since cells gradually increase in size from the periphery to the interior of the endosperm (27), we focused our investigation regions on ten cell layers, from the 3rd to the 12th cell layer neighboring the aleurone layer, to quantify endosperm cell size and cell number. We obtained similar average cell sizes in *dek701* and WT endosperm (Figure 6E and F). However, cell number in *dek701* endosperm was about 50% lower than that in WT, which mainly accounted for the difference of endosperm size between WT and *dek701* (Figure 6G).

Fewer cells are always correlated with slower cell-cycle progression and lower cell-proliferation activity (62). To assess the possible influence of the *dek701* mutation on the cell cycle, we determined the DNA contents of nuclei (C value) from 15-DAP WT and *dek701* endosperm using flow cytometry (Figure 6H and I). The 3C peak was the tallest in both WT and *dek701*, followed by peaks of decreasing intensity with progressively higher C numbers (from 6C to 96C in WT; from 6C to 48C in *dek701*) (Figure 6H). The relative proportions of DNA peaks were different between the two genotypes: 3C nuclei represented about 50.7% of the total DNA contents in *dek701* endosperm, but only reached 26.7% in WT. As the 3C peak is indicative of nuclei in the G1 phase of mitosis (63), the higher 3C peak in *dek701* relative to WT indicated that the cell cycle is arrested at the G1 phase in *dek701* (Figure 6I).

Cell proliferation is generally regulated by plant hormones (64,65). GO analysis in this study revealed the change in hormone signaling in *dek701* kernels. We thus quantified the contents of endogenous phytohormones in 15 DAP kernels (seed coat removed) by ultra-performance liquid chromatography–tandem mass spectrometry (LC-MS/MS). Levels of ABA, MeJA and brassinosteroids increased significantly, while those of IAA and GA_4 decreased, in *dek701* compared to the WT ($P < 0.05$ or $P < 0.01$; Figure 6J).

DEK701 interacts with ZmRPABC2 in the RNA pol machinery

Different subunits are assembled into RNAP through direct or indirect interactions (66,67). We identified 69 genes encoding putative RNAP subunits in the maize genome (Supplemental Table S1), of which we cloned 25 genes to test whether they could interact with DEK701 in a yeast two-hybrid (Y2H) assay. We established that DEK701 can interact with the common subunit ZmRPABC2a1 (GRMZM2G086904) and ZmRPABC2a2 (GRMZM2G013600) (Figure 7A and Supplemental Figure S9). Luciferase complementation image (LCI) and bimolecular fluorescence complementation (BiFC) assays confirmed the interaction of these proteins, as the co-infiltration of *N. benthamiana* leaves with the relevant LCI or BiFC constructs harboring *Dek701* and *ZmRPABC2a1* or *ZmRPABC2a2* resulted in strong luciferase activity (LCI) and YFP fluorescence signal (BiFC) (Figure 7B and C). Furthermore, BiFC assays allowed us to localize the site of interaction to the nucleus and the cytoplasm (Figure 7C), which was consistent with the subcellular localization of DEK701 (Figure 3E and F). These results confirm that DEK701 can directly interact with ZmRPABC2.

DISCUSSION

DEK701 is a core subunit of RNAPs and interacts with ZmRPABC2

All types of RNAPs are composed of multiple subunits to form each holoenzyme, with individual subunits exerting different functions. Prokaryotic RNAPs contain five core subunits: β, β', α, α and ω (8–10). Eukaryotic Pol I, II and III contain 10 core subunits. In this study, we identified DEK701 as a core subunit of maize Pol I, II and III, whose loss of function disrupted the activity of all RNAPs, resulting in the altered abundance of mRNA, tRNA, rRNA and ncRNA. We detected an interaction between DEK701 and ZmRPABC2 by Y2H assay but failed to detect a comparable interaction between DEK701 and other RNAP subunits (Figure 7A; Supplemental Figure S9). LCI and BiFC assays confirmed the interaction between DEK701 and ZmRPABC2 *in vivo* (Figure 7B and C). ZmRPABC2 is also a common subunit of RNAPs whose loss of function in maize generated a defective kernel phenotype similar to that seen in *dek701*, strongly suggesting that ZmRPABC2 might share a similar function with ZmRPABC5.

Research from yeast showed that RPABC5 is present at the periphery of all three RNA Pols (68–70) and interacts not only with the two essential subunits Rpac40 (RPB3) and Rpac19 (RPB11) of Pol II but also with the two largest subunits Rpa190 (RPB1) and Rpa135 (RPB2) of Pol I (71,72). Likewise, human RPABC5 (RPB10β) interacts strongly with RPB3 and weakly with RPB1, RPB2 and RPABC1 of Pol I, as well as with RPB7 and RPABC3 of Pol II (73). In contrast to the yeast and human reports mentioned above, the Arabidopsis RPABC5 (RPB10) subunit only interacts with NRPC3 (a Pol III-specific subunit homologous to the non-core prokaryotic subunit C82) (74). We established here that DEK701 (ZmRPABC5b) only interacts with ZmRPABC2, which is similar to the results

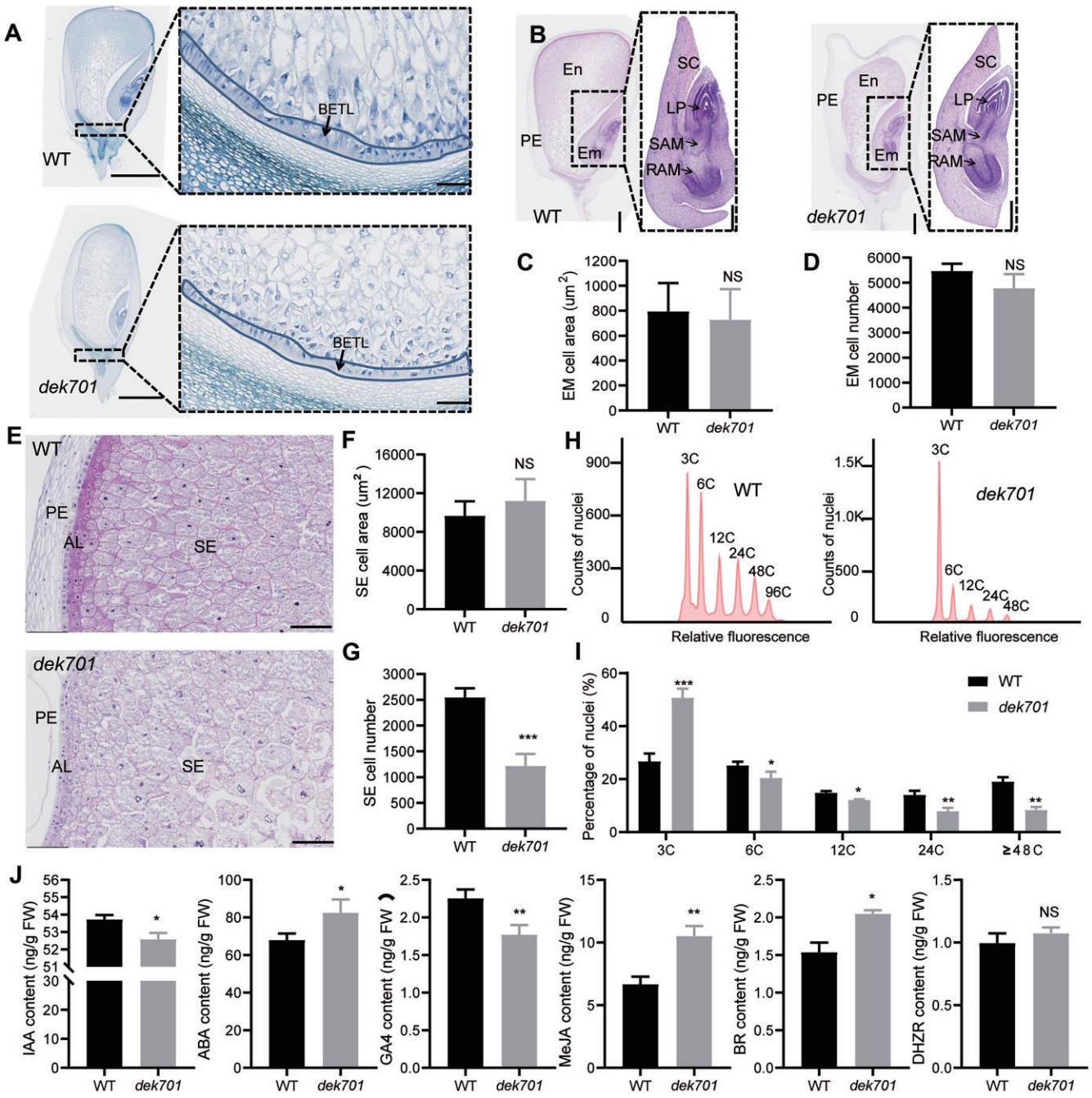

Figure 6. Cell proliferation features and phytohormone concentrations in WT and *dek701* kernels. (**A**) Basal endosperm transfer layer cells in longitudinal paraffin sections of WT sibling and *dek701* endosperm at 16 DAP. Scale bars = 2.5 mm. The right panels provide a higher magnification of the boxed areas; scale bars = 100 μm. (**B**) Longitudinal paraffin sections of WT sibling and *dek701* embryos from the same segregating ear at 21 DAP. Scale bars = 1 mm (500 μm in magnified pictures). (C, D) Total area of the developing embryo (EM) (**C**) and total EM cell number (**D**) in 20-DAP WT sibling and *dek701* kernels. Values are means ± SD ($n = 3$; NS, no significant difference at $P < 0.05$ as determined by Student's *t*-test). (**E**) Longitudinal paraffin sections of WT sibling and *dek701* endosperm from the same segregating ear at 20 DAP. SE, starchy endosperm; SG, starch granule; AL, aleurone layer; PE, pericarp. Scale bars = 200 μm. (F, G) Total area of the developing endosperm (EN) (**F**) and total EN cell number (**G**) in 20-DAP WT sibling and *dek701* kernels. Values are means ± SD ($n = 3$; $^{***}P < 0.001$; NS, no significant difference as determined by Student's *t*-test), which were recorded from the 3rd to 12th layer of endosperm cells neighboring the aleurone layer. (H, I) Flow cytometry profiles of WT sibling and *dek701* endosperm nuclei at 16 DAP. (**H**) Distribution of relative nuclear DNA contents (in relative fluorescence intensity) obtained by flow cytometry. The corresponding C values are indicated for each peak. (**I**) Histogram of DNA contents in WT sibling and *dek701* endosperm. Values are means ± SD ($n = 3$; $^{*}P < 0.05$; $^{**}P < 0.01$; $^{***}P < 0.001$ as determined by Student's *t*-test). (**J**) Phytohormone concentrations in 16-DAP WT sibling and *dek701* kernels (seed coat removed). IAA, indole-3-acetic acid; IPA, isopentenyl adenosine; ZR, zeatin riboside; ABA, abscisic acid; GA_4, gibberellic acid 4; JA, jasmonic acid; BR, brassinolide. Data are means ± SD ($n = 3$; $^{*}P < 0.05$; $^{**}P < 0.01$; NS, no significant difference as determined by Student's *t*-test).

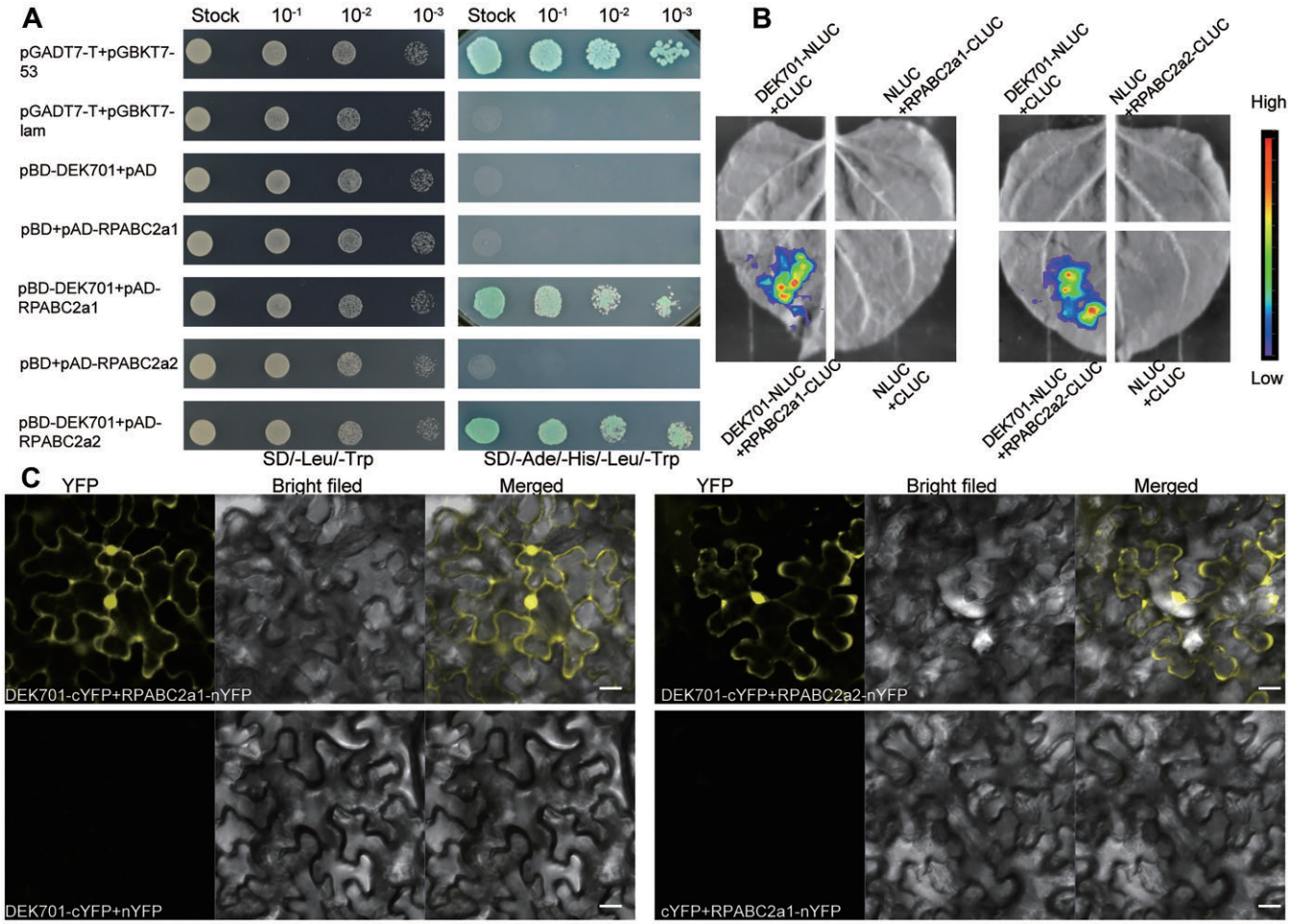

Figure 7. Interaction analysis between DEK701 and ZmRPABC2. (**A**) Y2H assay showing the interaction between DEK701, ZmRPABC2a1 and ZmRPABC2a2. The plasmids pGADT7-T (pAD-T) and pGBKT7-53 (pBD-53) served as positive controls; pAD-T and pGBKT7-Lam (pBD-Lam) served as negative controls. (**B**) LCI analysis in *N. benthamiana* leaves for the indicated pairs of constructs. Luminescence signal intensity represents interaction strength. (**C**) BiFC assay in *N. benthamiana* leaves for the indicated pairs of constructs. YFP fluorescence was detected by confocal microscopy 48 h after infiltration. Scale bars = 20 μm.

obtained in Arabidopsis. These results thus suggest that RPABC5 may interact with distinct subunits in different eukaryotic species and that the assembly of RNAPs might vary between species. False positive or false negative results may stem from limitations associated with conducting interaction tests in a heterologous system such as assays, so we cannot exclude the possibility that DEK701 might interact with other RNAP subunits.

RNAPs are central hubs for the regulation of endosperm development in maize

The endosperm makes up about 80–90% of the total kernel weight in maize, thus greatly contributing to seed weight and to grain yield in cereal crops (75,76). Since the identification of the maize mutant (*o2*) defective in endosperm development, endosperm development has been shown to be influenced by a wide range of biological pathways and their related proteins, such as respiration and mitochondrial proteins, the ubiquitin pathway, nutrient biosynthesis and metabolism, and regulators of transcription (26,77). Recently, Zhao (19) reported the first cloning of the Pol III-specific subunit gene *NRPC2* that regulates Pol III activity and endosperm development in maize, underscoring the important roles of Pol III in endosperm development. Here, we cloned *Dek701* encoding a common subunit of Pol I, II and III and demonstrated that its genetic inactivation leads to lower transcription levels of most RNAs, including rRNAs, mRNAs, tRNAs and lncRNAs, resulting in the arrest of maize endosperm development (Figure 5). Our results thus confirm the important roles played by RNAP in regulating maize endosperm development.

We determined that the *dek* phenotype in *dek701* mainly results from fewer cells and lower starch contents in the endosperm (Supplemental Figure S4B; Figure 6G). In general, a smaller cell number is related to slower or impaired cell-cycle progression (78). The *dek701* mutant exhibited an altered cytometry profile relative to WT, with a much lower proportion of duplicated nuclei with C values of 6C or greater (Figure 6H and I), confirming that the cell cycle is affected in *dek701*. A similar cytometry phenotype was also reported in the maize mutant with loss of NRPC2

function (19). As 6C reflect duplicated intermediate DNA contents of nuclei (63), the mutations of *Dek701* and *ZmRPABC2* might affect the cell cycle by blocking DNA replication at the G1–S phase. The cell cycle is controlled by cyclin-dependent kinases (CDKs), which are either activated by cyclins and cell division cycle proteins or repressed by CDK inhibitors (79). The expression of *CDK* genes was not affected in *dek701* compared to WT (Supplemental Data Set S2), indicating that the observed cell-cycle arrest in *dek701* might result from dysregulation of a pathway that does not involve the transcription of cell cycle–related genes. Mutations in the RNA Pol C (III)-specific subunit RPC53 in yeast and rice, RPC2 in zebrafish and Polr3b in mice cause a delay in the G1–S transition (12–14,17), indicating that dysfunction of Pol III, rather than Pol II, might lead to the cell cycle phenotypes detected in *dek701*. RNAP can function as a primase that generates small RNAs used as primers for the initiation of DNA replication (80–83), raising the possibility that the lower biosynthesis of small RNAs resulting from the defect in Pol III function as in *dek701* might explain the impaired DNA duplication and cell-cycle progression of the mutant during endosperm development.

Phytohormone signaling plays critical roles in the control of endosperm development. Auxin is a main contributor in regulating endosperm development (84–87). Auxin content in maize increases at the beginning of endoreduplication and remains at high levels throughout kernel development (88,89). ABA also regulates many developmental processes in plants, including seed development and germination (90,91). In individual Arabidopsis knockdowns of the RNA Pol subunits *NRPC2*, *NRPC3*, *NRPC8*, *NRPABC1*, and *NRPABC2*, the most common DEGs are enriched in the biosynthesis and signaling of phytohormones such as ABA, auxin and jasmonic acid (74). In this work, loss of DEK701 function resulted in lower IAA contents in maize kernels and affected the expression of nine ABA signal transduction genes and 24 auxin signal transduction genes, with 11 genes encoding repressors of auxin signaling being upregulated. Consistent with these changes in transcript levels, we detected the altered contents for IAA and ABA in *dek701* kernels, compared to WT (Figure 6J). These results suggest that the loss of Pol II activity in the *dek701* mutant changes the expression of genes related to auxin signaling, thus inhibiting auxin signaling and endoreduplication, ultimately leading to the lower cell number seen in *dek701*.

During the grain filling period of maize, grain volume increases rapidly and the endosperm synthesizes a large amount of nutrients for storage. In maize kernels, starch and proteins account for ∼70% and ∼10% of the total kernel weight, respectively (92). Interaction of the maize Fl3 protein with RNA Pol III subunit RPC53 affects the transcription of tRNA and 5S rRNA during endosperm development and storage reserve filling (18). Downregulated genes in the *fl3* mutants were enriched in genes encoding storage protein and starch biosynthesis enzymes related to nutrient reservoir activity, which was accompanied by lower starch and total protein contents in the *fl3* mutant compared to the WT. These results thus demonstrate the critical role of the Fl3-mediated modulation of RNAP III function in endosperm nutrient storage. In this study, GO terms associated with nutrient reservoir activity (GO:0045735) and carbohydrate metabolism (GO:0005975) included 16 and 118 DEGs, respectively. Most of these genes were downregulated in *dek701* compared to WT, which is consistent with the lower accumulation of reserves in *dek701* kernels, suggesting that DEK701 contributes to storage reserve accumulation. However, the maize *nrpc2* mutant did not affect nutrient storage capacity (19). These results thus illustrate the common and unique features of different RNAP subunits, providing a novel entry point to understand the function of individual subunits.

Taken together, the results of this study show that RNAP acts as a central hub for regulating endosperm development in maize, through the coordinated interplay of the cell cycle, transcription, phytohormone signaling and nutrient metabolism.

The Opaque2–*Dek701* transcriptional regulatory module controls maize endosperm development

Opaque2 directly regulates multiple genes for storage reserve accumulation during seed development, by directly binding to the Opaque2 box or a GCN4 motif within the promoter of its target genes (46,93,94). Using RNA-seq and chromatin immunoprecipitation followed by deep sequencing, Zhan (95) identified 186 putative direct Opaque2 targets, among which RNAP subunit genes were notably not included. Opaque2 transactivates *Sucrose synthase1* (*Sus1*) and *Sus2* transcription to enhance import of sugars from source organs to the developing seed for protein and starch biosynthesis during endosperm filling (96). In addition, Opaque2 directly binds to the *ZmGRAS11* promoter to activate its transcription to promote cell expansion in the filling endosperm (97). In the *o2* endosperm, expression of *Dek701* was about two-fold lower than that in WT (Figure 4E), indicating that *Dek701* might be a target of Opaque2.

RPABC5 is highly conserved in all investigated species, from yeast to plants and animals (Figure 3A). We checked digital expression data for rice, sorghum, and *B. distachyon*: in all species, *RPABC5a* was highly expressed in endosperm, whereas its ortholog *RPABC5b* was almost not expressed or expressed to very low levels (Supplemental Table S2). Although *ZmRPABC5a* expression is also high in maize, *Dek701* (*ZmRPABC5b*) expression levels were significantly higher than those of *ZmRPABC5a*, especially in seeds (Figure 3C and D). The *Dek701* promoter contained a unique GCN4 *cis*-element that is missing from the promoters of its rice, sorghum, and *B. distachyon* paralogs. We hypothesize that the highly specific expression of *Dek701* in maize endosperm is likely due to Opaque2 regulation via binding to the GCN4 element (Figure 4B and C), which was supported by the Y1H and EMSA results and the identification of a strong *cis*-eQTL in the *Dek701* promoter region mapping only 435 bp away from the GCN4 motif (Figure 4A). *cis*-eQTLs are generally under negative selection (98,99), although some *cis*-eQTLs have been subjected to positive selection for the upregulation of their cognate genes (100). There is a SNP (S_164712777) located within the Opaque2 binding motif (TGTGTCAT) of *Dek701*. Analysis of the allele frequencies of the SNP in maize Hapmap3 panel, which consists 1111 maize lines and 20 teosinte lines, showed that

T allele was significantly enriched in maize sub-population when comparing with teosinte sub-population. Furthermore, the allele frequencies of the SNP in another independent resource panel, which consists 507 maize lines and 70 teosinte lines, showed more significant enrichment of T allele in maize sub-population (Supplemental Figure S10). Therefore, on a population genetic scale, the upregulation of *Dek701* probably resulted from strong artificial selection on the upstream *cis*-regulatory region of *Dek701* during the domestication of maize, and the Opaque2–*Dek701* transcriptional regulatory module might be specific in maize to control endosperm development.

DATA AVAILABILITY

The data underlying this article are available in the article and in its online supplementary data. The RNA-seq data are available from the National Center for Biotechnology Information Gene Expression Omnibus (www.ncbi.nlm.nih.gov/geo) under the series entry PRJNA792688.

SUPPLEMENTARY DATA

Supplementary Data are available at NAR Online.

ACKNOWLEDGEMENTS

Yj.L., J.W., and R.G. designed the research. Q.C., Y.G., Y.L., J.W., X.D. and L.L. performed the research. Q.C., J.Z., J.L., S.Z. and J.F. analyzed the data. Yj.L., J.W., R.G. and Q.C. wrote the article.We thank Plant Editors (https://planteditors.com/) for manuscript editing, and Dr Rentao Song from China Agricultural University for providing the *o2* mutant.

FUNDING

National Natural Sciences Foundation of China [32072130]; key project at central government level: the ability establishment of sustainable use for valuable Chinese medicine resources [2060302]; National Natural Sciences Foundation of China [32072129]; Modern Agro-Industry Technology Research System of Maize [CARS-02-13]. Funding for open access charge: National Natural Sciences Foundation of China.
Conflict of interest statement. None declared.

REFERENCES

1. Nudler,E. (1999) Transcription elongation: structural basis and mechanisms. *J. Mol. Biol.*, **288**, 1–12.
2. von Hippel,P.H. (1998) An integrated model of the transcription complex in elongation, termination, and editing. *Science*, **281**, 660–665.
3. Schramm,L. and Hernandez,N. (2002) Recruitment of RNA polymerase III to its target promoters. *Genes Dev.*, **16**, 2593–2620.
4. Woychik,N.A. and Hampsey,M. (2002) The RNA Polymerase II Machinery: structure Illuminates Function. *Cell*, **108**, 453–463.
5. Grummt,I. (2003) Life on a planet of its own: regulation of RNA polymerase I transcription in the nucleolus. *Genes Dev.*, **17**, 1691–1702.
6. Hirata,A., Klein,B.J. and Murakami,K.S. (2008) The X-ray crystal structure of RNA polymerase from Archaea. *Nature*, **451**, 851–854.
7. Vassylyev,D.G., Sekine,S., Laptenko,O., Lee,J., Vassylyeva,M.N., Borukhov,S. and Yokoyama,S. (2002) Crystal structure of a bacterial RNA polymerase holoenzyme at 2.6 Å resolution. *Nature*, **417**, 712–719.
8. Ebright,R.H. (2000) RNA polymerase: structural similarities between bacterial RNA polymerase and eukaryotic RNA polymerase II. *J. Mol. Biol.*, **304**, 687–698.
9. Werner,F. (2007) Structure and function of archaeal RNA polymerases. *Mol. Microbiol.*, **65**, 1395–1404.
10. Wild,T. and Cramer,P. (2012) Biogenesis of multisubunit RNA polymerases. *Trends Biochem. Sci.*, **37**, 99–105.
11. Cramer,P., Armache,K.-J., Baumli,S., Benkert,S., Brueckner,F., Buchen,C., Damsma,G.E., Dengl,S., Geiger,S.R., Jasiak,A.J. *et al.* (2008) Structure of eukaryotic RNA polymerases. *Annu. Rev. Biophys.*, **37**, 337–352.
12. Mann,C., Micouin,J.Y., Chiannilkulchai,N., Treich,I., Buhler,J.M. and Sentenac,A. (1992) RPC53 encodes a subunit of *Saccharomyces cerevisiae* RNA polymerase C (III) whose inactivation leads to a predominantly G1 arrest. *Mol. Cell. Biol.*, **12**, 4314–4326.
13. Kieckhaefer,J.E., Lukovac,S., Ye,D.Z., Lee,D., Beetler,D.J., Pack,M. and Kaestner,K.H. (2016) The RNA polymerase III subunit Polr3b is required for the maintenance of small intestinal crypts in mice. *Cell. Mol. Gastroenterol. Hepatol.*, **2**, 783–795.
14. Yee,N.S., Gong,W., Huang,Y., Lorent,K., Dolan,A.C., Maraia,R.J. and Pack,M. (2007) Mutation of RNA Pol III subunit rpc2/polr3b leads to deficiency of subunit Rpc11 and disrupts Zebrafish digestive development. *PLoS Biol.*, **5**, e312.
15. Zhang,Q.-Q., Li,Y., Fu,Z.-Y., Liu,X.-B., Yuan,K., Fang,Y., Liu,Y., Li,G., Zhang,X.-S., Chong,K. *et al.* (2018) Intact Arabidopsis RPB1 functions in stem cell niches maintenance and cell cycling control. *Plant J.*, **95**, 150–167.
16. Chen,L., Guan,L., Qian,P., Xu,F., Wu,Z., Wu,Y., He,K., Gou,X., Li,J. and Hou,S. (2016) NRPB3, the third largest subunit of RNA polymerase II, is essential for stomatal patterning and differentiation in Arabidopsis. *Development*, **143**, 1600–1611.
17. Wang,A., Hou,Q., Si,L., Huang,X., Luo,J., Lu,D., Zhu,J., Shangguan,Y., Miao,J., Xie,Y. *et al.* (2019) The PLATZ transcription factor GL6 affects grain length and number in rice. *Plant Physiol.*, **180**, 2077–2090.
18. Li,Q., Wang,J., Ye,J., Zheng,X., Xiang,X., Li,C., Fu,M., Wang,Q., Zhang,Z. and Wu,Y. (2017) The maize imprinted gene *Floury3* encodes a PLATZ protein required for tRNA and 5S rRNA transcription through interaction with RNA polymerase III. *Plant Cell*, **29**, 2661–2675.
19. Zhao,H., Qin,Y., Xiao,Z., Li,Q., Yang,N., Pan,Z., Gong,D., Sun,Q., Yang,F., Zhang,Z. *et al.* (2020) Loss of function of an RNA polymerase III subunit leads to impaired maize kernel development. *Plant Physiol.*, **184**, 359–373.
20. Woychik,N.A., Liao,S.M., Kolodziej,P.A. and Young,R.A. (1990) Subunits shared by eukaryotic nuclear RNA polymerases. *Genes Dev.*, **4**, 313–323.
21. Woychik,N.A. and Young,R.A. (1993) RNA polymerase II subunit RPB10 is essential for yeast cell viability. *J. Biol. Chem.*, **268**, 12230.
22. Gontarek,B.C., Neelakandan,A.K., Wu,H. and Becraft,P.W. (2016) NKD transcription factors are central regulators of maize endosperm development. *Plant Cell*, **28**, 2916–2936.
23. Feng,F., Qi,W., Lv,Y., Yan,S., Xu,L., Yang,W., Yuan,Y., Chen,Y., Zhao,H. and Song,R. (2018) OPAQUE11 is a central hub of the regulatory network for maize endosperm development and nutrient metabolism. *Plant Cell*, **30**, 375–396.
24. He,Y., Wang,J., Qi,W. and Song,R. (2019) Maize *Dek15* encodes the cohesin-loading complex subunit SCC4 and is essential for chromosome segregation and kernel development. *Plant Cell*, **31**, 465–485.
25. Huang,Y., Wang,H., Huang,X., Wang,Q., Wang,J., An,D., Li,J., Wang,W. and Wu,Y. (2019) Maize VKS1 regulates mitosis and cytokinesis during early endosperm development. *Plant Cell*, **31**, 1238–1256.
26. Dai,D., Ma,Z. and Song,R. (2021) Maize kernel development. *Mol. Breeding*, **41**, 2.
27. Chen,Q., Zhang,J., Wang,J., Xie,Y., Cui,Y., Du,X., Li,L., Fu,J., Liu,Y., Wang,J. *et al.* (2021) Small kernel 501 (*smk501*) encodes the RUBylation activating enzyme E1 subunit ECR1 (E1 C-TERMINAL RELATED 1) and is essential for multiple aspects

of cellular events during kernel development in maize. *New Phytol.*, **230**, 2337–2354.
28. Chen,W., Cui,Y., Wang,Z., Chen,R., He,C., Liu,Y., Du,X., Liu,Y., Fu,J., Wang,G. *et al.* (2021) Nuclear-encoded maturase protein 3 is required for the splicing of various group II introns in mitochondria during maize (*Zea mays* L.) seed development. *Plant Cell Physiol.*, **62**, 293–305.
29. Pedroza-Garcia,J.A., Eekhout,T., Achon,I., Nisa,M.-U., Coussens,G., Vercauteren,I., Van den Daele,H., Pauwels,L., Van Lijsebettens,M., Raynaud,C. *et al.* (2021) Maize ATR safeguards genome stability during kernel development to prevent early endosperm endocycle onset and cell death. *Plant Cell*, **33**, 2662–2684.
30. Wallace,J.C., Lopes,M.A., Paiva,E. and Larkins,B.A. (1990) New methods for extraction and quantitation of zeins reveal a high content of γ-zein in modified opaque-2 maize. *Plant Physiol.*, **92**, 191–196.
31. Smith,P.K., Krohn,R.I., Hermanson,G.T., Mallia,A.K., Gartner,F.H., Provenzano,M.D., Fujimoto,E.K., Goeke,N.M., Olson,B.J. and Klenk,D.C. (1985) Measurement of protein using bicinchoninic acid. *Anal. Biochem.*, **150**, 76–85.
32. Bradford,M.M. (1976) A rapid and sensitive method for the quantitation of microgram quantities of protein utilizing the principle of protein-dye binding. *Anal. Biochem.*, **72**, 248–254.
33. Liu,S., Yeh,C.-T., Tang,H.M., Nettleton,D. and Schnable,P.S. (2012) Gene mapping via bulked segregant RNA-Seq (BSR-Seq). *PLoS One*, **7**, e36406.
34. Lei,Y., Lu,L., Liu,H.-Y., Li,S., Xing,F. and Chen,L.-L. (2014) CRISPR-P: a web tool for synthetic single-guide RNA design of CRISPR-system in plants. *Mol. Plant*, **7**, 1494–1496.
35. Xing,H.-L., Dong,L., Wang,Z.-P., Zhang,H.-Y., Han,C.-Y., Liu,B., Wang,X.-C. and Chen,Q.-J. (2014) A CRISPR/Cas9 toolkit for multiplex genome editing in plants. *BMC Plant Biol.*, **14**, 327.
36. Liu,Y., Zhang,Y., Liu,Y., Lu,W. and Wang,G. (2015) Metabolic effects of glyphosate on transgenic maize expressing a *G2-EPSPS* gene from *Pseudomonas fluorescens*. *J. Plant Biochem. Biotechnol.*, **24**, 233–241.
37. Yoo,S.-D., Cho,Y.-H. and Sheen,J. (2007) Arabidopsis mesophyll protoplasts: a versatile cell system for transient gene expression analysis. *Nat. Protoc.*, **2**, 1565–1572.
38. Lin,R., Ding,L., Casola,C., Ripoll,D.R., Feschotte,C. and Wang,H. (2007) Transposase-derived transcription factors regulate light signaling in Arabidopsis. *Science*, **318**, 1302–1305.
39. Chen,H., Zou,Y., Shang,Y., Lin,H., Wang,Y., Cai,R., Tang,X. and Zhou,J.-M. (2007) Firefly luciferase complementation imaging assay for protein-protein interactions in plants. *Plant Physiol.*, **146**, 368–376.
40. Song,S., Qi,T., Huang,H., Ren,Q., Wu,D., Chang,C., Peng,W., Liu,Y., Peng,J. and Xie,D. (2011) The jasmonate-ZIM domain proteins interact with the R2R3-MYB transcription factors MYB21 and MYB24 to affect jasmonate-regulated stamen development in Arabidopsis. *Plant Cell*, **23**, 1000–1013.
41. Lu,Q., Tang,X., Tian,G., Wang,F., Liu,K., Nguyen,V., Kohalmi,S.E., Keller,W.A., Tsang,E.W.T., Harada,J.J. *et al.* (2009) Arabidopsis homolog of the yeast TREX-2 mRNA export complex: components and anchoring nucleoporin: TREX-2 mRNA export complex. *Plant J.*, **61**, 259–270.
42. Trapnell,C., Pachter,L. and Salzberg,S.L. (2009) TopHat: discovering splice junctions with RNA-Seq. *Bioinformatics*, **25**, 1105–1111.
43. Trapnell,C., Williams,B.A., Pertea,G., Mortazavi,A., Kwan,G., Van,M.B., Salzberg,S.L., Wold,B.J. and Pachter,L. (2010) Transcript assembly and quantification by RNA-Seq reveals unannotated transcripts and isoform switching during cell differentiation. *Nat. Biotechnol.*, **28**, 511–515.
44. Trapnell,C., Roberts,A., Goff,L., Pertea,G., Kim,D., Kelley,D.R., Pimentel,H., Salzberg,S.L., Rinn,J.L. and Pachter,L. (2012) Differential gene and transcript expression analysis of RNA-seq experiments with TopHat and Cufflinks. *Nat. Protoc.*, **7**, 562–578.
45. Li,L., Eichten,S.R., Shimizu,R., Petsch,K., Yeh,C.-T., Wu,W., Chettoor,A.M., Givan,S.A., Cole,R.A., Fowler,J.E. *et al.* (2014) Genome-wide discovery and characterization of maize long non-coding RNAs. *Genome Biol.*, **15**, R40.
46. Li,C., Qiao,Z., Qi,W., Wang,Q., Yuan,Y., Yang,X., Tang,Y., Mei,B., Lv,Y., Zhao,H. *et al.* (2015) Genome-wide characterization of cis-acting DNA targets reveals the transcriptional regulatory framework of Opaque2 in Maize. *Plant Cell*, **27**, 532–545.
47. Doležel,J., Greilhuber,J. and Suda,J. (2007) Estimation of nuclear DNA content in plants using flow cytometry. *Nat. Protoc.*, **2**, 2233–2244.
48. Paterson,A.H., Bowers,J.E. and Chapman,B.A. (2004) Ancient polyploidization predating divergence of the cereals, and its consequences for comparative genomics. *Proc. Natl. Acad. Sci. U.S.A.*, **101**, 9903–9908.
49. Tello-Ruiz,M.K., Naithani,S., Gupta,P., Olson,A., Wei,S., Preece,J., Jiao,Y., Wang,B., Chougule,K., Garg,P. *et al.* (2021) Gramene 2021: harnessing the power of comparative genomics and pathways for plant research. *Nucleic Acids Res.*, **49**, D1452–D1463.
50. Wang,L., Beissinger,T.M., Lorant,A., Ross-Ibarra,C., Ross-Ibarra,J. and Hufford,M.B. (2017) The interplay of demography and selection during maize domestication and expansion. *Genome Biol.*, **18**, 215.
51. Huang,C., Sun,H., Xu,D., Chen,Q., Liang,Y., Wang,X., Xu,G., Tian,J., Wang,C., Li,D. *et al.* (2018) ZmCCT9 enhances maize adaptation to higher latitudes. *Proc. Natl. Acad. Sci. USA*, **115**, E334–E341.
52. Guo,L., Wang,X., Zhao,M., Huang,C., Li,C., Li,D., Yang,C.J., York,A.M., Xue,W., Xu,G. *et al.* (2018) Stepwise *cis*-regulatory changes in ZCN8 contribute to maize flowering-time adaptation. *Curr. Biol.*, **28**, 3005–3015.
53. Yang,X., Gao,S., Xu,S., Zhang,Z., Prasanna,B.M., Li,L., Li,J. and Yan,J. (2011) Characterization of a global germplasm collection and its potential utilization for analysis of complex quantitative traits in maize. *Mol. Breeding*, **28**, 511–526.
54. Fu,J., Cheng,Y., Linghu,J., Yang,X., Kang,L., Zhang,Z., Zhang,J., He,C., Du,X., Peng,Z. *et al.* (2013) RNA sequencing reveals the complex regulatory network in the maize kernel. *Nat. Commun.*, **4**, 2832.
55. Yang,N., Liu,J., Gao,Q., Gui,S., Chen,L., Yang,L., Huang,J., Deng,T., Luo,J., He,L. *et al.* (2019) Genome assembly of a tropical maize inbred line provides insights into structural variation and crop improvement. *Nat. Genet.*, **51**, 1052–1059.
56. Kellogg,E.A. (2001) Evolutionary History of the Grasses1. *Plant Physiol.*, **125**, 1198–1205.
57. Freeling,M. (2009) Bias in plant gene content following different sorts of duplication: tandem, whole-genome, segmental, or by transposition. *Annu. Rev. Plant Biol.*, **60**, 433–453.
58. Wu,C.-Y., Suzuki,A., Washida,H. and Takaiwa,F. (1998) The GCN4 motif in a rice glutelin gene is essential for endosperm-specific gene expression and is activated by Opaque-2 in transgenic rice plants. *Plant J.*, **14**, 673–683.
59. Albani,D., Hammond-Kosack,M.C., Smith,C., Conlan,S., Colot,V., Holdsworth,M. and Bevan,M.W. (1997) The wheat transcriptional activator SPA: a seed-specific bZIP protein that recognizes the GCN4-like motif in the bifactorial endosperm box of prolamin genes. *Plant Cell*, **9**, 171–184.
60. Bukowski,R., Guo,X., Lu,Y., Zou,C., He,B., Rong,Z., Wang,B., Xu,D., Yang,B., Xie,C. *et al.* (2018) Construction of the third-generation *Zea mays* haplotype map. *GigaScience*, **7**, gix134.
61. Kelley,D.R. and Estelle,M. (2012) Ubiquitin-mediated control of plant hormone signaling. *Plant Physiol.*, **160**, 47–55.
62. Brioudes,F., Thierry,A.-M., Chambrier,P., Mollereau,B. and Bendahmane,M. (2010) Translationally controlled tumor protein is a conserved mitotic growth integrator in animals and plants. *Proc. Natl. Acad. Sci. U.S.A.*, **107**, 16384–16389.
63. Schweizer,L., Yerk-Davis,G.L., Phillips,R.L., Srienc,F. and Jones,R.J. (1995) Dynamics of maize endosperm development and DNA endoreduplication. *Proc. Natl. Acad. Sci. U.S.A.*, **92**, 7070–7074.
64. Takatsuka,H. and Umeda,M. (2014) Hormonal control of cell division and elongation along differentiation trajectories in roots. *J. Exp. Bot.*, **65**, 2633–2643.
65. Chandler,J.W. and Werr,W. (2015) Cytokinin–auxin crosstalk in cell type specification. *Trends Plant Sci.*, **20**, 291–300.
66. Young,R.A. (1991) RNA Polymerase II. *Annu. Rev. Biochem.*, **60**, 689–715.
67. Kuznedelov,K., Minakhin,L., Niedziela-Majka,A., Dove,S.L., Rogulja,D., Nickels,B.E., Hochschild,A., Heyduk,T. and

Severinov,K. (2002) A Role for Interaction of the RNA Polymerase Flap Domain with the σ Subunit in Promoter Recognition. *Science*, **295**, 855–857.
68. Cramer,P., Bushnell,D.A. and Kornberg,R.D. (2001) Structural basis of transcription: RNA polymerase II at 2.8 Ångstrom resolution. *Science*, **292**, 1863–1869.
69. Fernández-Tornero,C., Moreno-Morcillo,M., Rashid,U.J., Taylor,N.M.I., Ruiz,F.M., Gruene,T., Legrand,P., Steuerwald,U. and Müller,C.W. (2013) Crystal structure of the 14-subunit RNA polymerase I. *Nature*, **502**, 644–649.
70. Hoffmann,N.A., Jakobi,A.J., Moreno-Morcillo,M., Glatt,S., Kosinski,J., Hagen,W.J.H., Sachse,C. and Müller,C.W. (2015) Molecular structures of unbound and transcribing RNA polymerase III. *Nature*, **528**, 231–236.
71. Lalo,D., Carles,C., Sentenac,A. and Thuriaux,P. (1993) Interactions between three common subunits of yeast RNA polymerases I and III. *Proc. Natl. Acad. Sci. U.S.A.*, **90**, 5524–5528.
72. Flores,A., Briand,J.-F., Gadal,O., Andrau,J.-C., Rubbi,L., Mullem,V.V., Boschiero,C., Goussot,M., Marck,C., Carles,C. *et al.* (1999) A protein–protein interaction map of yeast RNA polymerase III. *Proc. Natl. Acad. Sci. U.S.A.*, **96**, 7815–7820.
73. Acker,J., Graaff,M.d., Cheynel,I., Khazak,V., Kedinger,C. and Vigneron,M. (1997) Interactions between the human RNA polymerase II subunits. *J. Biol. Chem.*, **272**, 16815–16821.
74. Zhao,H., Qin,Y., Xiao,Z., Liang,K., Gong,D., Sun,Q. and Qiu,F. (2021) Knockdown NRPC2, 3, 8, NRPABC1 and NRPABC2 affects RNAPIII activity and disrupts seed development in Arabidopsis. *Int. J. Mol. Sci.*, **22**, 11314.
75. Kowles,R.V. and Phillips,R.L. (1988) Endosperm development in maize. In: Bourne,G.H., Jeon,K.W. and Friedlander,M. (eds.) *International Review of Cytology*. Academic Press, Vol. **112**, pp. 97–136.
76. Song,X.-J., Huang,W., Shi,M., Zhu,M.-Z. and Lin,H.-X. (2007) A QTL for rice grain width and weight encodes a previously unknown RING-type E3 ubiquitin ligase. *Nat. Genet.*, **39**, 623–630.
77. Dai,D., Ma,Z. and Song,R. (2021) Maize endosperm development. *J. Integr. Plant Biol.*, **63**, 613–627.
78. Giacinti,C. and Giordano,A. (2006) RB and cell cycle progression. *Oncogene*, **25**, 5220–5227.
79. Sabelli,P.A. and Larkins,B.A. (2009) The Development of endosperm in grasses. *Plant Physiol.*, **149**, 14–26.
80. Brutlag,D., Schekman,R. and Kornberg,A. (1971) A possible role for RNA polymerase in the initiation of M13 DNA synthesis. *Proc. Natl. Acad. Sci. U.S.A.*, **68**, 2826–2829.
81. Wickner,W., Brutlag,D., Schekman,R. and Kornberg,A. (1972) RNA synthesis initiates *in vitro* conversion of M13 DNA to its replicative form. *Proc. Natl. Acad. Sci. U.S.A.*, **69**, 965–969.
82. Masai,H. and Arai,K. (1996) Mechanisms of primer RNA synthesis and D-loop/R-loop-dependent DNA replication in *Escherichia coli*. *Biochimie*, **78**, 1109–1117.
83. Khan,S.A. (2005) Plasmid rolling-circle replication: highlights of two decades of research. *Plasmid*, **53**, 126–136.
84. Lau,S., Slane,D., Herud,O., Kong,J. and Jürgens,G. (2012) Early embryogenesis in flowering plants: setting up the basic body pattern. *Annu. Rev. Plant Biol.*, **63**, 483–506.
85. Figueiredo,D.D., Batista,R.A., Roszak,P.J. and Köhler,C. (2015) Auxin production couples endosperm development to fertilization. *Nat. Plants*, **1**, 15184.
86. Robert,H.S., Park,C., Gutièrrez,C.L., Wójcikowska,B., Pěnčík,A., Novák,O., Chen,J., Grunewald,W., Dresselhaus,T., Friml,J. *et al.* (2018) Maternal auxin supply contributes to early embryo patterning in Arabidopsis. *Nat. Plants*, **4**, 548–553.
87. Figueiredo,D.D. and Köhler,C. (2018) Auxin: a molecular trigger of seed development. *Genes Dev.*, **32**, 479–490.
88. Lur,H.S. and Setter,T.L. (1993) Role of auxin in maize endosperm development (timing of nuclear DNA endoreduplication, zein expression, and cytokinin). *Plant Physiol.*, **103**, 273–280.
89. Doll,N.M., Fargeix,N.D., Rogowsky,P.M. and Widiez,T. (2017) Signaling in early maize kernel development. *Mol. Plant*, **10**, 375–388.
90. Chinnusamy,V., Gong,Z. and Zhu,J.-K. (2008) Abscisic acid-mediated epigenetic processes in plant development and stress responses. *J. Integr. Plant Biol.*, **50**, 1187–1195.
91. Cutler,S.R., Rodriguez,P.L., Finkelstein,R.R. and Abrams,S.R. (2010) Abscisic acid: emergence of a core signaling network. *Annu. Rev. Plant Biol.*, **61**, 651–679.
92. Flint-Garcia,S.A., Bodnar,A.L. and Scott,M.P. (2009) Wide variability in kernel composition, seed characteristics, and zein profiles among diverse maize inbreds, landraces, and teosinte. *Theor. Appl. Genet.*, **119**, 1129–1142.
93. Washida,H., Wu,C.-Y., Suzuki,A., Yamanouchi,U., Akihama,T., Harada,K. and Takaiwa,F. (1999) Identification of *cis*-regulatory elements required for endosperm expression of the rice storage protein glutelin gene GluB-1. *Plant Mol. Biol.*, **40**, 1–12.
94. Li,C. and Song,R. (2020) The regulation of zein biosynthesis in maize endosperm. *Theor. Appl. Genet.*, **133**, 1443–1453.
95. Zhan,J., Li,G., Ryu,C.-H., Ma,C., Zhang,S., Lloyd,A., Hunter,B.G., Larkins,B.A., Drews,G.N., Wang,X. *et al.* (2018) Opaque-2 regulates a complex gene network associated with cell differentiation and storage functions of maize endosperm. *Plant Cell*, **30**, 2425–2446.
96. Deng,Y., Wang,J., Zhang,Z. and Wu,Y. (2020) Transactivation of *Sus1* and *Sus2* by Opaque2 is an essential supplement to sucrose synthase-mediated endosperm filling in maize. *Plant Biotechnol. J.*, **18**, 1897–1907.
97. Ji,C., Xu,L., Li,Y., Fu,Y., Li,S., Wang,Q., Zeng,X., Zhang,Z., Zhang,Z., Wang,W. *et al.* (2022) The O2-ZmGRAS11 transcriptional regulatory network orchestrates the coordination of endosperm cell expansion and grain filling in maize. *Mol. Plant*, **15**, 468–487.
98. Josephs,E.B., Lee,Y.W., Stinchcombe,J.R. and Wright,S.I. (2015) Association mapping reveals the role of purifying selection in the maintenance of genomic variation in gene expression. *Proc. Natl. Acad. Sci. U.S.A.*, **112**, 15390–15395.
99. Hernandez,R.D., Uricchio,L.H., Hartman,K., Ye,C., Dahl,A. and Zaitlen,N. (2019) Ultra-rare variants drive substantial cis-heritability of human gene expression. *Nat. Genet.*, **51**, 1349.
100. Kita,R., Venkataram,S., Zhou,Y. and Fraser,H.B. (2017) High-resolution mapping of cis-regulatory variation in budding yeast. *Proc. Natl. Acad. Sci. U.S.A.*, **114**, E10736–E10744.